ENGINEERING RESEARCH INSTITUTE
UNIVERSITY OF MICHIGAN
ANN ARBOR

PROGRESS REPORT NO. 4

WING-BODY INTERFERENCE

(Period covering February 1 to April 30, 1952)

By

R. E. PHINNEY

Projects M937 and M937-A

WRIGHT AIR DEVELOPMENT CENTER, U. S. AIR FORCE
CONTRACT AF 33(038)-19747, E. O. NO. 460-31-12-11 SR-1g

TABLE OF CONTENTS

LIST OF SYMBOLS USED

r,θ,z = cylindrical coordinates

M = free stream Mach number

$\alpha = \sqrt{M^2 - 1}$

R = radius of cylinder

$Z' = \frac{Z}{\alpha R} = \frac{1}{2}$ intersection distance

$r' = \frac{r}{R}$

Φ = velocity potential function for total flow

ϕ = velocity potential of the body due to interference effects

V_∞ = free stream velocity

δ = flow deflection angle through the shock wave

V_c = uniform cross-flow velocity due to shock wave = $V_\infty \sin \delta$

$\phi_n(r',z')$ = Fourier components ϕ

$v_n(z')$ = velocity normal to the surface of the body due to the shock wave

$a_n(z')$ = Fourier component amplitudes of V_n as a function of ϕ

f_n = Ferrari distribution function for ϕ

$\dot{f}_n$ = derivative of f_n with respect to its argument

$K_n^{(i)}$ = constant value of $\dot{f}_n$ in $i^{\underline{th}}$ interval

$L(\ ) = \int_0^\infty e^{-sz'}\ (\ )dz'$, Laplace transform with respect to z'

K_n = the modified Bessel function of the second kind of order n

W_n and M_n = characteristic functions

$\Gamma(\ )$ = ordinary gamma function

g_n = Nielson distribution function

s = variable in Laplace transform

LIST OF FIGURES

I. INTRODUCTION

This report contains a summary of the theoretical work which has been accomplished to date on the wing-body interaction study being carried out at the University of Michigan Supersonic Wind Tunnel under Contract AF 33(038)-19747. One of the objectives of this program is to investigate the overall flow field at Mach No. 1.90 over the combined configuration of a cylindrical fuselage and the inner portion of a thin wing of triangular section and to investigate the results in terms of existing nonviscous wing-body interference theories in order to try to assess the viscous effects in the actual case. Thus the purpose is not only to check linearized theory but also to use it as a basis to "subtract out", if possible, the nonviscous effects so that an idea of the purely viscous effects can be obtained. As a preliminary step in this investigation the especially simple (from the point of view of getting a mathematical solution) case of a plane shock wave intersecting a cylindrical body has been studied using the three different methods of (1) Ferrari (Ref.1), (2) Nielsen-Matteson (Ref.2), and (3) Nielson (Ref.3). (See pp. 5-13 for a short discussion of these methods).

There are two reasons for choosing the shock-wave—cylinder problem mentioned above for a preliminary study. First, this case is simple in that the first step in the iteration process normally needed to solve a wing-body problem up to and after the trailing edge of the wing (see pp. 3-4 for further discussion) yields the final solution, since we assume that the shock-generating wedge ("wing") is at infinity so that any interference effects from the cylinder ("body") reflecting from the wedge back to the cylinder will influence the cylinder only infinitely far downstream. Secondly, there exist some experimental results for this case (Ref. 8) which may be compared to the theoretical results of the three methods mentioned above to get some idea of how much the theory and experiment can be expected to diverge.

Having computed the pressure distributions by the above-mentioned methods, it is possible to compare them with each other, especially with regard to:

(1) the computational time required;

(2) the difficulty of the computations involved, i.e., how much is straightforward computation and how many steps there are (many short ones or a few long straightforward ones);

(3) the extent to which the various methods are sensitive to computing errors or approximations, i.e., are errors accumulative;

(4) the accuracy of the methods both at the intersection of the shock wave and the cylinder and also assymptotically in z, i.e., to what extent do the discontinuities in the boundary conditions effect the accuracy of the solution; and

(5) the extent to which general statements can be made concerning the solution, i.e., can the rate with which the solution reaches its assymptotic value be determined or can integrated effects be determined readily.

II. GENERAL DISCUSSION OF LINEARIZED THEORY

Physically the supersonic wing-body interference problem consists of attempting to find the changes in pressure on the body of a missile or aircraft caused by the proximity of the wing and, conversely, to find the change in pressure on the wing due to the presence of the body. In order to render the problem tractable, it is necessary to make several assumptions at the outset. First, we must eliminate the viscosity from the equations of motion. Even the flow over quite simple configurations cannot be solved exactly if the viscosity is taken into consideration. Secondly, it is necessary to linearize the equations of motion after the viscosity has been set equal to zero. There are, to be sure, methods for handling problems concerned with simple configurations using the full nonlinear equations of motion, but these methods are difficult even in the case of a simple configuration. We will therefore consider from here on only linearized nonviscous isentropic irrotational flows over the wing-body configuration.

Certain other mathematical idealizations or approximations concerning the boundaries of the body are also introduced, namely, (1) that the surface of the body is a circular cylinder or that it is so nearly cylindrical that it can be so approximated; and (2) that although the wing

is twisted or at an angle of attack, it is still very close to a plane passing through the axis of the body, so that instead of satisfying the wing boundary conditions on the actual surface of the wing we will specify them in this plane.

The mathematical problem which confronts us, then, is that of finding the solution of the potential equation,

$$(M^2 - 1)\frac{\partial^2 \Phi}{\partial z^2} = \frac{1}{r^2}\frac{\partial^2 \Phi}{\partial \theta^2} + \frac{1}{r}\frac{\partial \Phi}{\partial r} + \frac{\partial^2 \Phi}{\partial r^2} \qquad (1)$$

with boundary conditions which give the normal derivative of Φ (velocity normal to the surface) on all parts of the wing and body and also the specification that there be no upstream influence of the wing-body juncture.

It should be noted here that we desire a detailed picture of the altered pressure distribution. We are not primarily interested in the gross effect of the interaction, i.e., the effect of the body on such integrated quantities as the lift, drag, and moment of the wing or the integrated lift, drag, and moment induced on the body by the wing. Consequently, we are not interested in what would happen if either the wing or the body became vanishingly small; e.g., we are not concerned with slender-body theories.

In order to simplify the problem, we assume that the span of the wing is such that the influence of the tip of the wing is not felt in the region in which we are interested. The problem can be solved with the tip effect in it, but it considerably complicates the solution. Furthermore, we assume a wing with supersonic leading edge, in particular a straight unswept wing, in order to eliminate interaction between the upper surface and the lower surface of the wing.

The wing-body interaction problem may be simplified further into a leading-edge problem and a trailing-edge problem. In the leading-edge problem we are concerned only with the interaction in the region ahead of the juncture of the wing trailing edge and the body, so that we can assume, in effect, that the wing chord is infinite as far as points in front of the trailing edge are concerned. In the trailing-edge problem we are interested also in the flow behind the wing trailing edge, i.e., in the flow over the afterbody which is induced by a wing of finite chord.

The solution up to the trailing edge, although tedious, is straightforward in that the solution can be obtained explicitly as an infinite series. Since there can be no interaction between the region above the wing plane and the region below the wing plane, we may apply an extra symmetry condition which destroys once and for all any effect on the wing plane due

to the bodies' perturbation potential. On the other hand, if we are interested in the pressure distribution on the body at and aft of the trailing edge, this extra symmetry condition is not necessarily present, so that we must use an iteration process such as that described by Ferrari. This iteration is set up as follows: the wing is first solved alone in the free stream; then the body is introduced into the flow field of the wing in the uniform stream and a second perturbation field is computed to cancel the velocities induced at the body surface by the wing. This second perturbation field will now destroy the boundary condition on the wing, so that a third perturbation field must be introduced to cancel the velocities induced in the wing plane by the second perturbation field. The third perturbation field then destroys the boundary conditions on the body, so that a fourth perturbation field must be computed, etc. If this iteration process converges, as it must (as pointed out in Ref. 4, p. 37), then we will have a solution to any wing-body problem to which we apply the method. In general, only the first step of this iteration process can be performed without a tremendous amount of work. Hence, in practice the accuracy of the method depends on the accuracy of the first approximation.

In order to solve wing-body interaction problems, it is necessary to be able to find for wing alone and body alone potential functions which satisfy certain given boundary conditions. The wing potential can be determined by the methods summarized in Ref. 5 or the method of Ref. 1. The body potential, in which we are more interested here, may be obtained by several methods. A brief outline of three of these methods, Refs. 1, 2, and 3, is presented later. It was considered desirable to study the body potential solution a little more closely, since in the tests proposed to be made under this contract most of the pressure holes are on the body. The reason for this is that the body is perfectly cylindrical and is made so that it can move with respect to the wing, so that in effect the orifice holes can be made to appear to move on the body, thus giving a very fine pressure coverage on the body. Another reason for working on the body potential is that it is the solution for a three-dimensional body, which, being more difficult than a two-dimensional solution, is necessarily subject to more approximations and hence more inaccuracies, so that it was considered desirable to check the various methods against each other on the body to try to determine their relative merits.

The specific problem to which the three methods of approach discussed below have been applied is that of a plane shock wave impinging on a cylindrical body in a supersonic stream with cylindrical axis in the streamwise direction. The reasons the shock-cylinder problem was selected for study were the following: First, this problem presents all the essential features of a wing-body problem, but it is considerably simplified in that no iteration process is necessary, since the effects from the body are reflected back to the body (by the shock-generating wedge or "wing") only at an infinitely great distance downstream from the first intersection

of the shock and the cylinder. Also, note that no wing solutions are necessary, since the "wing" has been moved to infinity, so that it has an influence on the body but we do not need to consider the effect of the body on the wing. In addition, this problem produces a uniform cross-flow past the body which can be very easily computed (by incompressible-flow methods, since the cross-flow component is very much subsonic) and compared with the theories used here. Also, the local solution on the surface just behind the shock wave can be obtained by two-dimensional sweep-back theory similar to that of Refs. 6 and 7, so that these results at the intersection line also can be compared to the theories used here. Lastly, the shock-cylinder problem was selected because there are considerable experimental data on this problem (Ref. 8) which can be used partly as an experimental check on the theoretical work, partly as a preliminary trial ground to see how strong the viscous effects are here, and also to try to get some idea of the order of magnitude of the errors in the theory (at least locally, where Ref. 6 can be compared with linear theory).

The shock-wave-cylinder problem is in some ways a difficult test for the linearized theory. (1) Behind the shock wave there is a uniform cross-flow which produces an asymptotic pressure distribution (characterized by a doublet flow about a circle), in which the square terms in velocity must be used to compute the pressure, since if the only axial component of velocity is used then the pressure would be found to be constant around the surface. In this case, then, the effect of the square terms on the pressure must be felt; the question is how soon and how much? (2) Due to the cross-flow mentioned above, there is a considerable accumulation and thickening of the boundary layer as we move around the surface of the cylinder toward the lee side. The thicker boundary layer materially alters the pressure distribution by changing the displacement thickness, by shifting the pressure distribution by means of pressure propagation through the boundary layer, and by separation effects. (3) The last reason is that the shock wave from the wedge hits the body and reflects two-dimensionally, causing large Mach number and pressure variations, whereas if the wedge were on the body (if it were a bonafide wing) then these effects would be less severe, since the maximum local pressure changes would be approximately half as great.

III. SUMMARY OF THE METHODS USED

Before we launch into a discussion of the results of the methods used on the shock-cylinder problem, it is probably a good idea to give a short summary of the methods used. The discussion is necessarily not

complete but only an outline of the approaches; for a complete explanation see the original reports (Refs. 1, 2, and 3).

A. Nielsen-Matteson Method

A possible method of solving for a body potential would be to distribute singularities over the surface of the body and then determine the strength of the singularities in order to satisfy the boundary condition that the normal derivative be specified (the negative of the velocity that we are trying to cancel). In a nonplanar problem this is, however, not as easy as it sounds, because each singularity that we introduce produces a normal derivative to the surface, depending on the strength of the singularity, at all points in the downstream Mach cone. The normal velocity induced by the singularity alters the boundary condition at these downstream points so that instead of the singularity strength depending only on the local normal velocity, it depends also on the integration of all the upstream singularities, thus we get an integral equation for the distribution function. The integral equation cannot, in general, be solved exactly; the next best thing is to attempt an approximate solution.

The continuous distribution of singularities on the surface of the body can be approximated by assuming that the strength of the singularities is constant over a small but finite area of the surface. Thus, the whole surface of the body is approximated by a large number of small but finite surface elements. If these small surface elements are now approximated by secant plane-surface elements, over which the strength of a supersonic source singularity is constant, we arrive at the physical picture described in Ref. 2, namely that each of the plane-surface elements is actually a plane symmetric wedge of finite span. In order to avoid the occurrence of infinite velocities on the surface of the body due to the infinite sidewash of the wedges, Ref. 2 places the wedges a small distance inside the cylinder.

In the method of Ref. 2, the surface of the body is divided into octagonal rings of length 0.4R (see Fig. 1). The average velocity normal to the surface of the cylinder was calculated by integrating the velocity over the area and dividing by the area.

From the boundary conditions the slopes of the wedges on the first ring can be computed; then, knowing these slopes, the boundary conditions at the downstream stations can be modified to account for velocity induced normal to the surface of the cylinder by the wedges in the first ring. We can then go to the second ring and compute the wedge slopes there in a manner similar to that used at the first ring. Having the wedge slopes at the second ring, we can then correct the normal velocities at all the downstream stations as we did for the first ring. We proceed ring-by-ring,

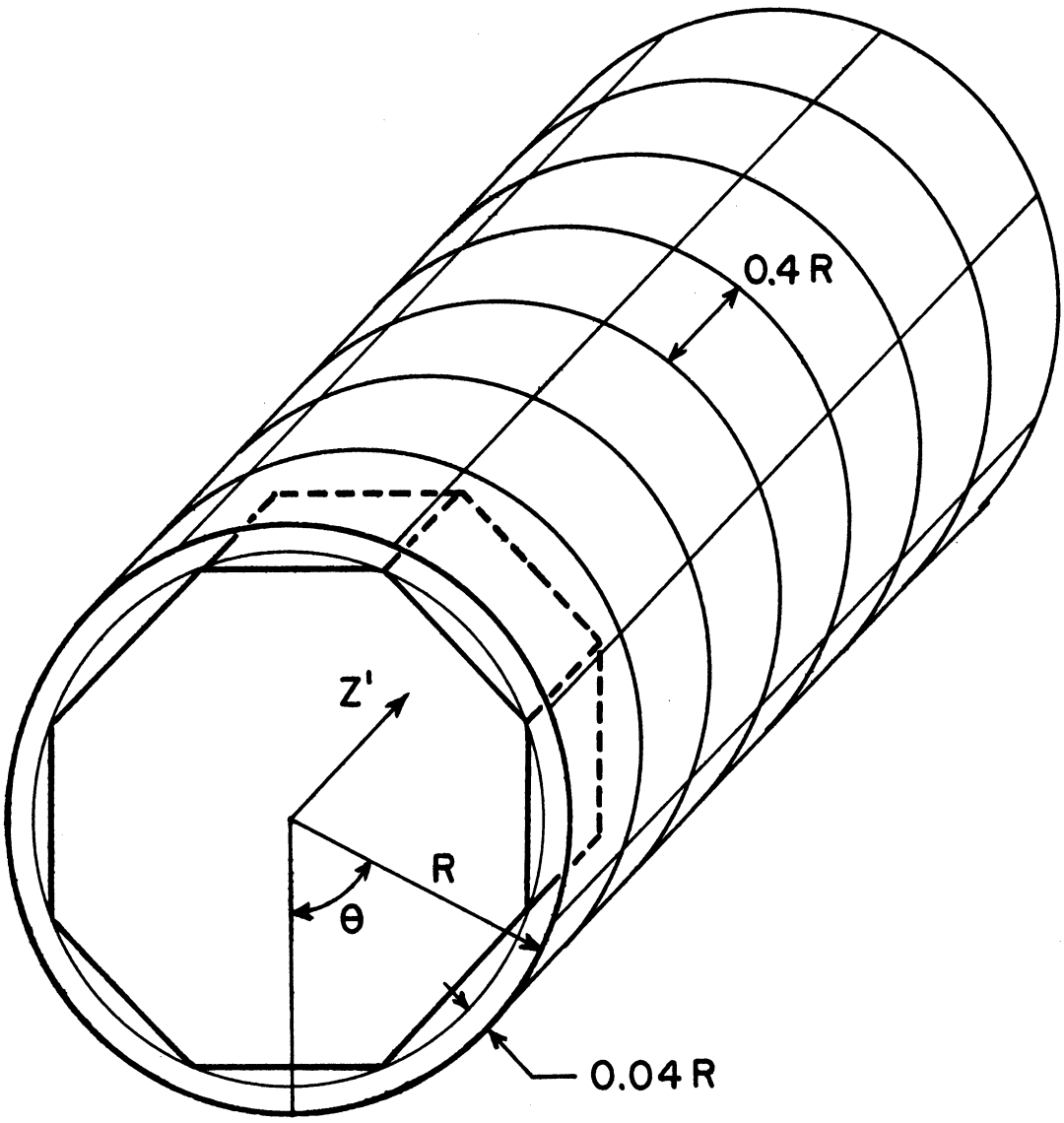

Fig.1 Octagonal Rings Used in the Nielsen – Matteson Theory.

downstream, finding wedge slopes and correcting boundary conditions at each successive ring until we have the wedge slopes as far downstream as we want them. With the solution for the wedge slopes, it is then possible to compute the velocity components anywhere in space by a simple superposition of the effects of all the wedges. In particular, we can find the velocity components on the surface of the cylindrical body, from which we can compute the pressure. In their report (Ref. 2), Nielsen and Matteson give tables for computing the wedge slopes from the average normal velocities to the areas and also a second table which gives the downstream influence of any given wedge on all the others that it affects.

B. Ferrari Method

The wing-body interaction problem is solved in Ref. 1 in a completely different manner from the Nielsen-Matteson approach. If we separate variables in Eq. 1, then the solution becomes:

$$\phi = V_c \sum_{n=0}^{\infty} \phi_n(r',z') \cos n\theta \quad , \tag{2}$$

where the terms containing sin $n\theta$ have been dropped because of symmetry with respect to the plane $\theta = 0$ (veritcal plane) and n is an integer due to the periodicity of ϕ in θ. It can be shown that to satisfy the potential equation, each of the ϕ_n must have an integral representation of the form

$$\phi_n(r',z') = \int_{\cosh^{-1}z'}^{0} f_n(z' - r' \cosh u) \cosh nu \, du \quad , \tag{3}$$

where f_n is an unknown distribution function to be determined by the boundary condition.

The boundary conditions $v_n(\theta,z')$ may be expanded in a Fourier series, with coefficients depending on Z':

$$V_n(\theta,z') = V_c \sum_{n=0}^{\infty} a_n(z') \cos n\theta \quad . \tag{4}$$

Differentiating Eq. 2 with respect to r' and setting r' = 1 gives us the velocity normal to the surface on the surface, which must cancel V_n as given in Eq. 4. Thus for each Fourier component we have

$$\left.\frac{\partial \phi_n(r',z')}{\partial r'}\right|_{r'=1} = -a_n(z') \quad . \tag{5}$$

Using the integral representation of ϕ_n given by Eq. 3, we have

$$-a_n(z') = \int_{\cosh^{-1}z'}^{0} f_n\,(z' - r' \cosh u) \cosh u \cosh nu\, du. \tag{6}$$

Since the integral equations (6) cannot be solved explicitly, Ref. 1 sets up a step-by-step procedure which is similar to that used by Von Karman and Moore (Ref. 13) and which gives the f_n's as a broken-line function. The procedure goes as follows:

(a) The z' axis is divided into a convenient number of equal intervals.

(b) The value of a_n in the first interval is used to find the slope, $K_n^{(1)}$, of f_n in the first interval.

(c) Then a_n at the end of the second interval and $K_n^{(1)}$ are used to find the slope, $K_n^{(2)}$, of f_n in the second interval. In general, $K_n^{(i)}$ can be determined in terms of a_n at the end of the $i^{\underline{th}}$ interval and all previous K_n's.

Once the distribution function f_n is known, ϕ_n may be obtained by a numerical evaluation of the integral appearing in Eq. 3. Once all the ϕ_n's are known the problem is solved.

C. Summary of Nielsen Method

The method of Ref. 3 is somewhat similar to that of Ref. 1. A separation of variables is performed on the wave equation so that the potential ϕ is again given by Eq. 2. Eq. 3, however, is replaced by

$$\phi_n = -\frac{1}{r'^n} \int_0^{z'-r'+1} g_n(\xi)\, \frac{\partial^{n-1}}{\partial \xi^{n-1}} \left[(z'-\xi+1)^2 - r'^2 \right]^{n-1/2} d\xi \,, \tag{7}$$

where $g_n(\xi)$ is the distribution function which corresponds to the f_n in Ref. 1 and

$$\frac{\partial^{n-1}}{\partial \xi^{n-1}} \left[(z' - \xi + 1)^2 - r'^2 \right]^{n-1/2}$$

is the singularity being distributed, which corresponds to cosh nu in Ref. 1. If we take the Laplace transformation of Eq. 7, we will get a fairly simple result, since the integral in that expression is of the convolution type so that the transformation $L(\phi_n)$ of ϕ_n becomes

$$L(\phi_n)\Big|_{r'=1} = - L(g_n) \frac{2^n \Gamma(n+\frac{1}{2})}{\sqrt{\pi}} \frac{e^s}{s} K_n(s). \tag{8}$$

We can also get another expression for $L(\phi_n)$ by transforming the differential equation and the boundary conditions; then, since the differential equation is an ordinary one, we can solve it explicitly. The transformed counterpart of Eq. 5 is

$$\frac{\partial}{\partial r'} \left[L(\phi_n) \right] \Big|_{r'=1} = - L(a_n) \tag{9}$$

and the transformation of the differential Eq. 1 is

$$\frac{\partial^2 \Phi}{\partial r'^2} + \frac{1}{r'} \frac{\partial \Phi}{\partial r'} + \frac{1}{r'^2} \frac{\partial^2 \Phi}{\partial \theta^2} - s^2 \Phi = 0 \quad . \tag{10}$$

Upon separating variables in Eq. 10, we can write the solution in the form

$$L(\Phi) = \sum_{n=0}^{\infty} C_n(s) K_n(sr') \quad , \tag{11}$$

or

$$L(\phi_n) = C_n(s) K_n(sr') \quad . \tag{12}$$

Differentiating Eq. 12 with respect to r', we get

$$\frac{\partial}{\partial r'} L(\phi_n) \Big|_{r'=1} = s c_n(s) K_n'(s) \quad . \tag{13}$$

Comparing this with Eq. 9, we can solve for the heretofore unknown coefficients $C_n(s)$ to get

$$C_n(s) = \frac{-L(a_n)}{sK_n'(s)} \tag{14}$$

Thus Eq. 12 can be written in the form

$$L(\phi_n)\Big|_{r'=1} = \frac{-L(a_n)\, K_n(s)}{s\, K_n'(s)} \quad . \tag{15}$$

Using Eqs. 15 and 8, we can solve for the Laplace transformation of g_n, the distribution function,

$$L(g_n) = \frac{\sqrt{\pi}}{2^n\, \Gamma(n+\frac{1}{2})} \left[sL(a_n) \right] \left[\frac{e^{-s}}{s\, K'(s)} \right] \quad . \tag{16}$$

If then we take the inverse transform we will have an explicit expression for the distribution function g_n. The right side, being a product of transforms, will become a convolution integral of the inverse transforms. If we define the inverse transform of the second factor to be a function $M_n(z')$, i.e.,

$$M_n(z') \equiv L^{-1} \left[\frac{e^{-s}}{s\, K'(s)} \right] \quad , \tag{17}$$

and if we note that the first factor is the transform of the derivative of a_n with respect to z', then we can write

$$g_n = \frac{2^n\, n!}{(2n)!} \int_0^{z'} a_n'(\xi)\, M_n(z'-\xi)\, d\xi \quad . \tag{18}$$

Having computed g_n, we are then in a position to substitute this in Eq. 7 and determine the velocity potential at any point in the field. The M_n functions are tabulated in Ref. 3 for even n up to $n = 6$. Expression 18 gives us essentially an inversion of the integral equation (6) of Ferrari, which removes the unknown distribution function from under the integral sign.

Nielsen has pointed out that if we are interested in the value of the axial velocity on the body only, then we do not need to find the distribution function, but rather we can get expressions that give us $d\phi_n/dx$ on

the surface directly in terms of an integration of the boundary conditions. To do this, simply take Eq. 15 and combine it with Eq. 20, which is a fundamental relation in Laplace transform theory,

$$L\left[\left.\frac{\partial \phi_n}{\partial z'}\right|_{r'=1}\right] = s\, L\left[\left.\phi_n\right|_{r'=1}\right] , \tag{20}$$

to get

$$L\left[\left.\frac{\partial \phi_n}{\partial z'}\right|_{r'=1}\right] = -s\, L\left[a_n\right] \frac{K_n(s)}{S\, K_n'(s)}$$

$$= L\left[a_n\right] - L\left[a_n\right]\left[\frac{K_n(s)+K_n'(s)}{K_n'(s)}\right] , \tag{21}$$

Now take the inverse transform of (21),

$$\left.\frac{\partial \phi_n}{\partial z'}\right|_{r'=1} = a_n - \int_0^{z'} a_n(\xi) W_n(z'-\xi)\, d\xi , \tag{22}$$

where

$$W_n(z) \equiv L^{-1}\left[\frac{K_n(s)+K_n'(s)}{K_n'(s)}\right] . \tag{23}$$

Having $\left.\frac{\partial \phi_n}{\partial z'}\right|_{r'=1}$, we can get the axial velocity perturbation and hence the linearized pressure, or we can integrate $\partial \phi_n/\partial z'$ with respect to z' and get ϕ_n as a function of z', which gives us the Fourier components of the tangential velocity.

The connection between the method of Ref. 2 and the methods of Refs. 1 and 3 can be demonstrated in the following intuitive manner. Ref. 2 distributes one kind of singularity, namely a supersonic source, on the surface of the cylinder, whereas Refs. 1 and 3 distribute an infinite variety of singularities on the axis of the cylinder. This is somewhat analogous to the solution of problems in ordinary potential theory, where this solution may be obtained either by a superposition of multipiles (harmonic functions) at the origin or by a surface distribution of singularities.

In addition to the methods described above there are two other reports, Refs. 9 and 10, that have some bearing on the problem being discussed, although these reports have not been applied specifically to the shock-wave-cylinder problem. Also, for a summary of methods of treating the wing-body problem in which the body is not necessarily a circular cylinder see Ref. 11.

IV. DISCUSSION OF COMPUTATIONS INVOLVED

Besides the linearization and the other usual approximations, each of the theories has some other approximations involved in order to bring the theory to a point where computations are possible.

A. Nielsen-Matteson Method

The approximations in the Nielsen-Matteson method are of quite a different sort from those in the other two methods. In this case the body has to be cut up into a set of finite areas over which the effects have to be averaged. The size of the areas that are used depends on a compromise between the accuracy desired and the time required for the computations. Octagonal rings of length 0.4R in the streamwise direction (see Fig. 1) were used in the computations for the shock-cylinder problem, since tables for the correction of boundary conditions and coefficients for computing the wedge slopes using this size of octagonal rings were already available in Ref. 2. The formulas necessary to compute the wedge slopes and the formulas to correct the normal velocity due to the effect of upstream wedges were easily generalized to the case where there is no symmetry between the upper and lower parts of the cylindrical body as is assumed in Ref. 2. The formulas were checked by assuming the symmetry property and verifying that the formulas then became the same as those in Ref. 2. In addition, it was necessary to compute tables for obtaining axial and tangential velocities from the wedge slopes.

It might be pointed out that the amount of time necessary for a calculation on a body with n rings varies roughly as n^2, since, for example, if we doubled the number of rings we would need to make twice as many corrections of the boundary conditions for the upstream wedges and since there are twice as many rings to do this for, there would be four times as many operations to perform.

The question of the size of the areas to be used for a certain accuracy is not too easy to answer, since it is a question not only of

how accurately the wedge slopes can be obtained from the boundary condition a particular ring but also of how accurately the boundary conditions have been corrected due to the influence of the upstream wedges.

One thing can be said, however, and that is the tangential velocities are not as accurate as the axial velocity components. This is a result of the fact that the wedges used to produce the interference velocities have infinite sideflow velocities at the tips which do not cancel because the surface of the adjacent wedges are not parallel and the strength of the singularities are not the same, since the neighboring wedges do not in general have the same slope. These infinities will affect both the normal and tangential velocities, but they will most strongly affect the tangential velocities.

The wedge sideflows are nearly tangent to the surface; in the limiting case they would be tangent and the neighboring wedges would have the same strength, so that the infinities of adjacent wedges would then cancel each other. In order to eliminate as far as possible the effects of the sideflows on the normal (as well as tangential) velocities, Nielsen and Matteson place the wedges a short distance inside the body, so that the infinite velocities are removed from the surface (see Fig. 1). The effect on the accuracy of the method caused by this displacement of the wedges from the surface is probably much less than the effect of averaging the velocities over an area in order to use wedges of finite size. At one station ($z' = 4.0$) the edge of the wedge was placed at distances of 0.02, 0.04, and 0.06 times the radius of the cylinder from the surface, and the ratios of average normal to average axial velocity were computed (this ratio determines what pressure will be induced on the surface due to a given normal velocity to be canceled); the ratios were found to be 0.87, 0.83, and 0.79 respectively. In Ref. 2 and in the computation for the shock-cylinder problem, the distance was taken as 0.04R.

In the application of the Nielsen-Matteson theory it was observed that although one would expect an asymptotic doublet flow around the cylinder some distance aft of the shock wave, the method did not seem able to produce this. The wedge slopes that were computed did not appear to converge as rings further and further downstream on the cylinder. Fig. 2 is a graph of the total wedge slopes as a function of z', the axial distance. As a consequence of this apparent lack of convergence of the wedge slopes, the velocities and pressures did not approach their asymptotic values. On the other hand, the method gives good results near the wing-leading-edge body juncture.

The probable explanation for the divergence of the wedge slopes is that the wedge areas are too large. When we average the boundary conditions over the area in which the boundary conditions vary quite strongly (for example, near the shock wave where the slope can be zero over part of

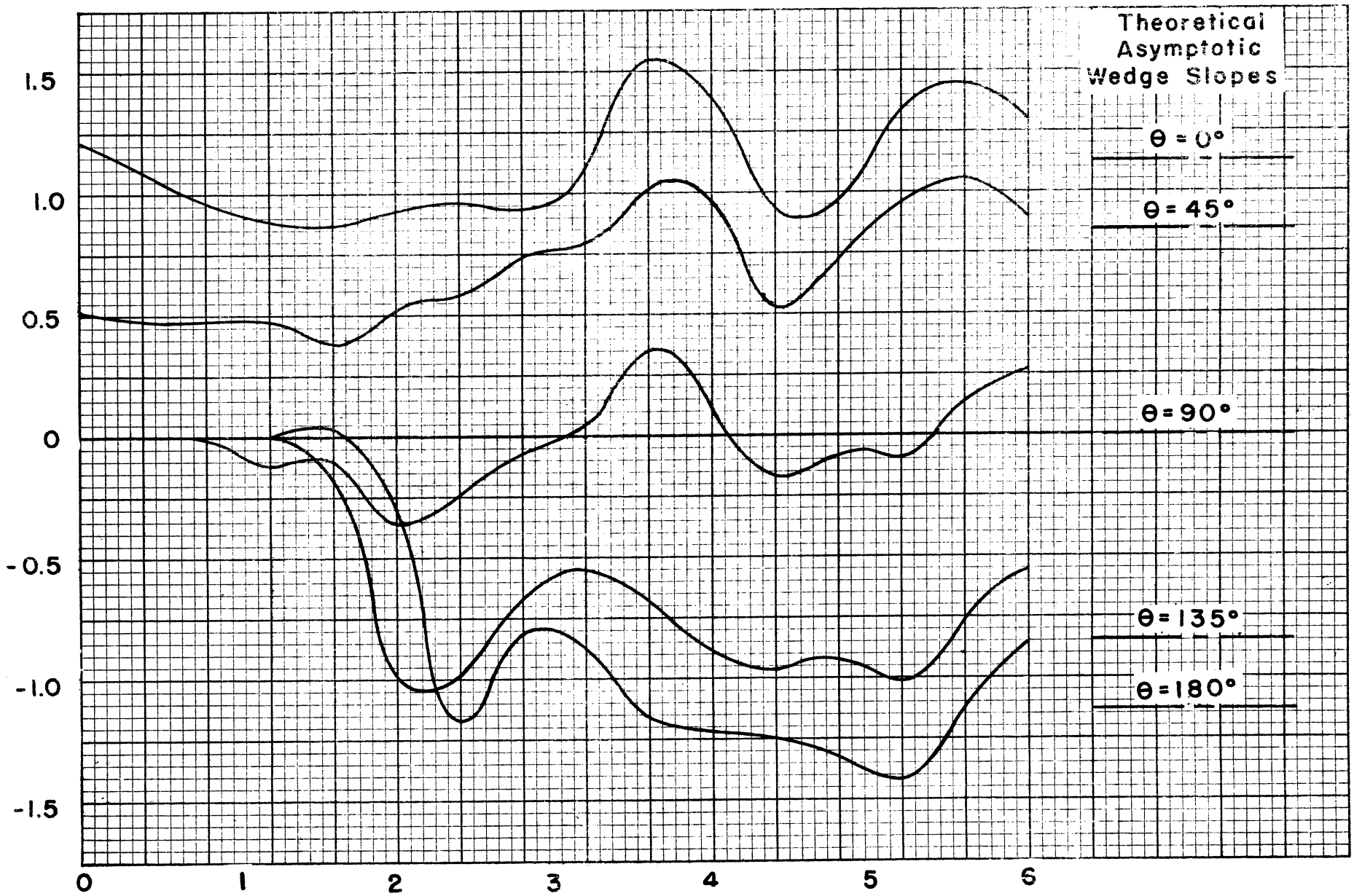

Fig. 2 Axial Distribution of Wedge Slopes – Nielsen-Matteson Method.

the area ahead of the shock line and something else over the rest of the area) and then determine an average wedge slope, we will of course have sizeable differences between this average wedge slope and the slopes of the smaller wedges which we would have obtained if we had broken the area up into finer divisions. If we consider the effect of this wedge on the following ones we will see that the average effect on the next area can vary somewhat with the manner in which the boundary conditions were canceled on the preceeding wedge (either on the average over the area or exactly at each point). Since each succeeding wedge slope has an influence on wedge slope to be solved for subsequently, any error in the first wedge slope will affect the second, and then the first and the second will affect the third and so forth, each error having a cumulative effect on downstream wedge slopes.

The Nielsen-Matteson theory has the advantage that it is easy to set up and once it has been put in a form for computation these computations are straightforward and easy to perform, the time needed to complete the method being about the same as for the other two methods.

B. Ferrari Method

Since the Ferrari method uses an expansion of the boundary condition in a Fourier series in Θ with coefficients depending on z', we will have the usual difficulties involved in approximating a step function with a finite number of terms from the infinite Fourier series.

The mathematical boundary condition is the given velocity normal to the body produced by the shock wave. If we nondimensionalize this normal velocity with respect to the uniform cross-flow of the shock, then v_n/V_c is equal to cos Θ, since v_n is just the component of the cross-flow V_c which is along the normal to the cylinder behind the shock plane and v_n is zero in front of the shock plane. We see at once that all the Fourier components will be zero in front of the shock and one intersection distance downstream they will all be zero again except for n=1 (the cos Θ term), which will remain 1 giving a doublet cross-flow in planes z' = const. Expanding the functions described above in the usual way, we obtain:

$$n\neq 1 \begin{cases} 0<z'<2 & a_n = \frac{1}{\pi} \dfrac{\sin\left[(n-1)\cos^{-1}(1-z')\right]}{n-1} + \frac{1}{\pi} \dfrac{\sin\left[(n-1)\cos^{-1}(1-z')\right]}{n+1} \\ z' \geq 2 & a_n = 0 \end{cases}$$

$$n=1 \begin{cases} 0<z'<2 & a_n = \dfrac{\cos^{-1}(1-z')}{\pi} + \frac{1}{2\pi} \sin\left[2\cos^{-1}(1-z')\right] \\ z'>2 & a_n = 1 \end{cases}$$

Fig. 3 is a graph showing the exact boundary conditions and the approximation to these exact boundary conditions if we retain only the first four terms in their Fourier series representation. Fig. 4 is a plot of the amplitudes of the Fourier components, $a_n(z')$. This plot may be used to determine roughly the number of terms necessary to give a certain approximation. The absolute magnitude of the terms behaves like $2/n\pi$ for large values of n. In addition, the frequency of oscillation of the components increases with increasing n, so that a finer division of increments along the z' axis is necessary in order to describe fully the contribution of the higher-order terms in the Fourier series. In the computations for the shock-cylinder configuration, only the first four terms were kept, because it was felt that this number of terms would give a sufficient amount of accuracy and yet not make the computational work excessive.

As mentioned previously, the Ferrari method involves the approximation of a continuous distribution function by a broken-line function. Furthermore, the slope of the distribution function in any one interval is a function of the slopes of the distribution function in all preceding intervals. As a result of this, any error in one interval may well have a cummulative effect, causing larger errors in downstream intervals. In the course of the computations it appeared that the approximations that were made did not seem to destroy the convergence, although computing errors of any size did introduce a sizeable error in the result. The computations involved in finding the distribution function are more complicated than the computations in the Nielsen-Matteson method, which were discussed in the previous section.

It should be noted that for each Fourier component the accuracy of the component depends on the fineness of the interval chosen and that for a given accuracy the interval used must be smaller for the higher-order components, since the higher-order boundary condition components fluctuate more rapidly, as previously pointed out. This permits the rapid calculation of the lower-order components using a large interval if only a rough approximation to the true answer is desired. In the course of the computations for f_1 in the shock-cylinder configuration, some trials were made using different interval lengths. The results indicate that the computations are quite insensitive to the internal size for ϕ_1. In fact, the full intersection distance was used for the interval length and even then the results were not far different from those obtained using one-fourth the intersection distance as the interval length.

Fig. 5 shows the various Fourier components ϕ_0, ϕ_1, ϕ_2, ϕ_3 of the interference velocity potential ϕ. In addition $\partial\phi_0/\partial z'$, $\partial\phi_1/\partial z'$, $\partial\phi_2/\partial z'$, and $\partial\phi_3/\partial z'$, which are involved in the computation of the axial perturbation velocity u', are shown in Fig. 5. $\partial\phi_i/\partial z'$ was obtained by analytically differentiating the expression for ϕ_i and then numerically integrating the

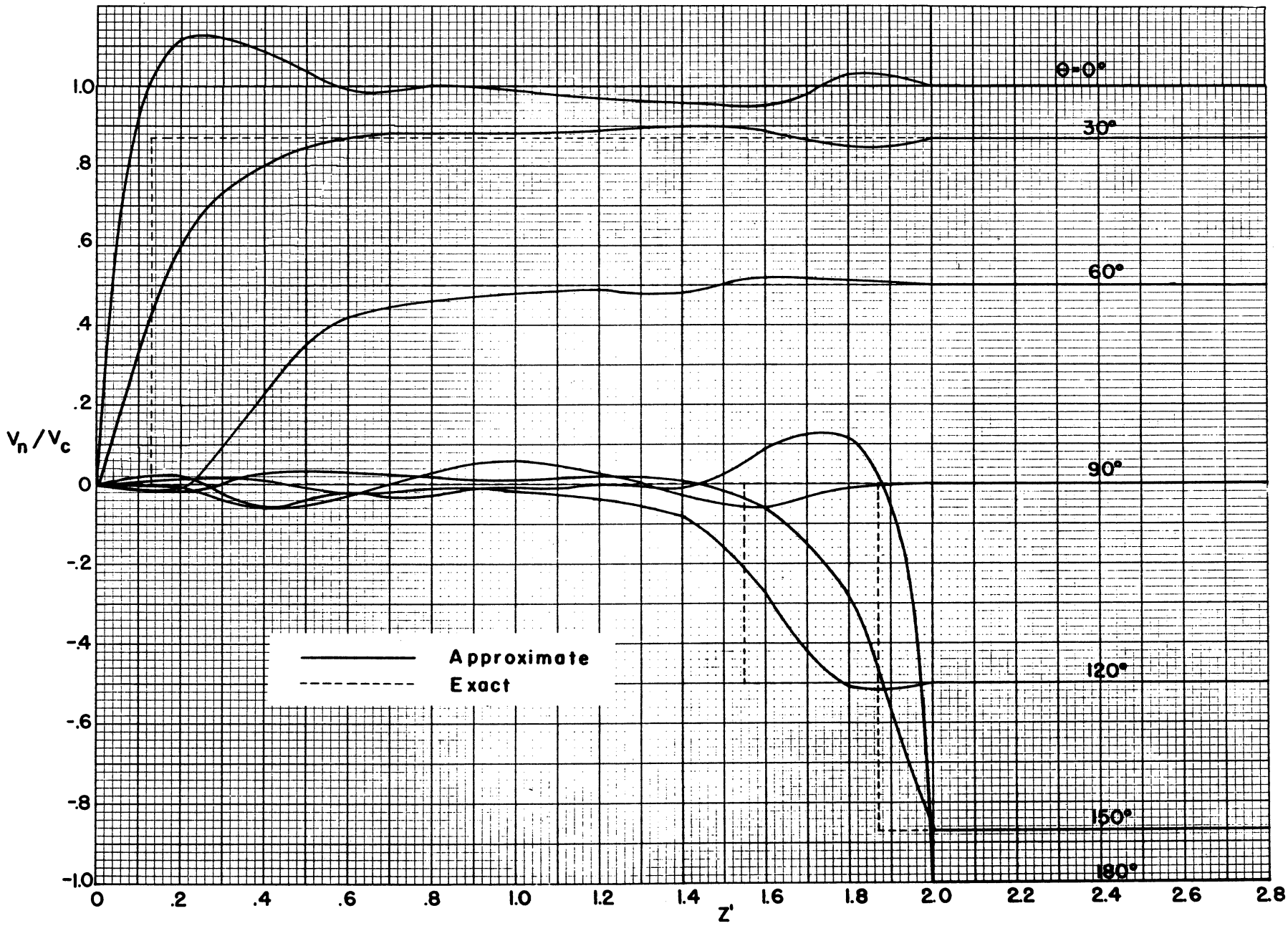

Fig. 3 Four Term Fourier Approximation to The Boundary Conditions at Various Meridional Sections.

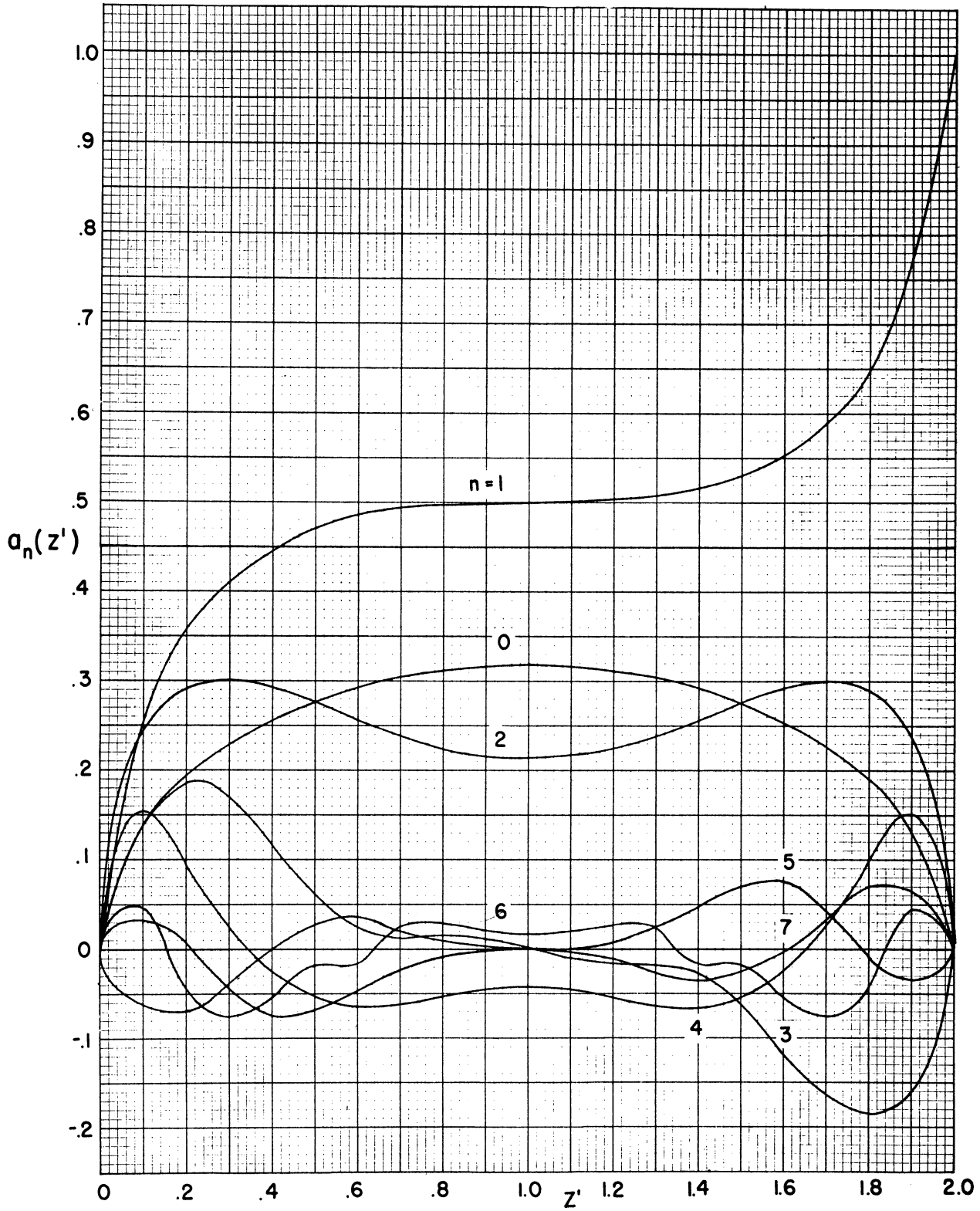

Fig. 4 Amplitude of Fourier Components For The Boundary Conditions.

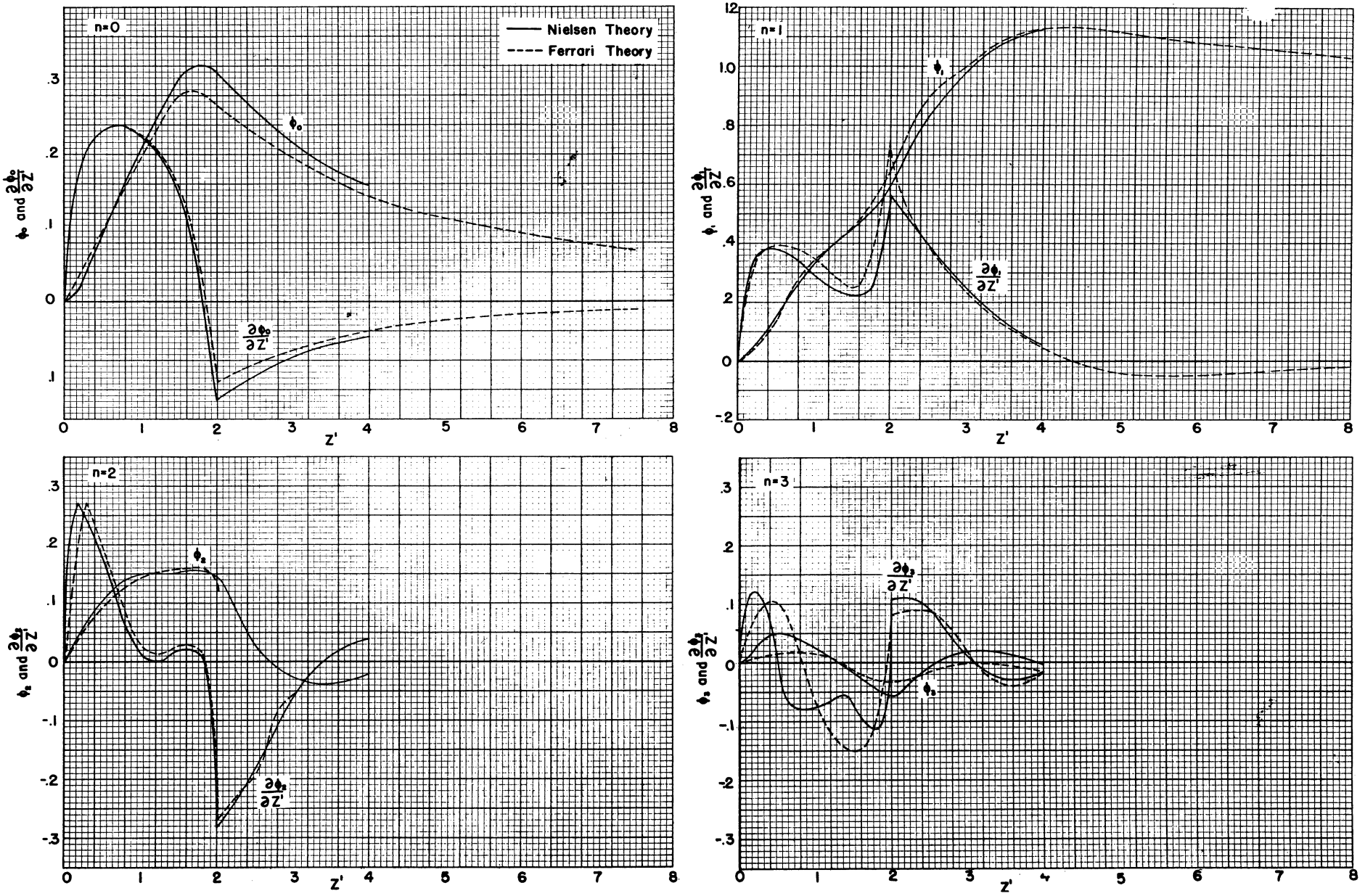

Fig 5. Fourier Components of ϕ_n and $\frac{\partial \phi_n}{\partial Z'}$ as Functions of Z'. $M=\sqrt{2}$

resulting expression, which involves only f's and K's. This procedure is preferable to simply differentiating the function $\phi_i(z_n')$ numerically, since it increases the accuracy of $\partial\phi_i/\partial z'$.

C. Nielsen Method

Since the first step in both the Nielsen method and the Ferrari method is a separation of the variable θ, the boundary conditions in both methods must be expressed in exactly the same way. Hence, all remarks made concerning the approximations involved in applying the boundary conditions in the Ferrari method, which were made in the previous section, apply equally well to the Nielsen method. In the present method the data necessary to solve the problem, the M and W functions, were available for all the even components up to the 6th, but none of the odd M's or W's were published, since, as pointed out before, in the usual case where we have independence of the upper and lower parts of the body a symmetry condition can be imposed which eliminates the odd-order terms. Since the W and M functions are defined as untabulated inverse Laplace transforms of combinations of Bessel functions, they are not too easy to compute and the difficulty of computation increases as n increases. Hence, only W_1 and W_3 were computed and their values are given in Appendix A. The error in W_1 and W_3 was kept to about 0.002. The corresponding M's were not computed, since we are interested here in the solution only on the surface of the body.

In the Nielsen as well as in the Ferrari method it can be observed that as the order of the component goes up more trouble can be expected in the solution. We note in Fig. 4 that as n gets larger the magnitude of a_n decreases as expected, but the number of fluctuations increases, so that if some approximate method is used to find the potential in which the value of a_n is assumed constant or linear in intervals, then in order to get a good approximation the size of the interval will have to be reduced for the larger values of n. Although values of $\partial\phi_n/\partial z'$ can be expressed as convolution integrals of the W_n functions and the boundary conditions, it is still necessary to preform the integrations numerically or graphically. The curve to be integrated has to be computed at a finite number of points a certain distance apart and then some form of numerical integration must be used. The accuracy of the results of course depends on the closeness of the points used in the numerical integration.

V. A BRIEF COMPARISON OF THE THREE METHODS

The Nielsen-Matteson theory has a certain advantage in that some physical interpretation can be put on almost all the steps in the solution.

Even though the Nielsen and Ferrari theories are less physical in their approach, they have certain other advantages from a computational viewpoint. In the Nielsen and Ferrari methods the basic problem is split up into a group of subproblems (one for each Fourier component), each of which is independent of the other subproblems, so that an error or a bad approximation in one subproblem will have no effect on the other parts of the solution. In the treatment of the subproblems the Ferrari method solves for a distribution function slope in such a way that the solution for each successive slope depends on all the preceding ones, which of course means that there is a possibility for a cumulative error to exist. However, it appeared in the actual solution that the approximation made in the first part of the solution did not seem to have any serious effect on the latter ones; that is, the process gave a solution that converged to the proper asymptotic values and compared very well with the Nielsen method, which uses an approach without this chance for a cumulative error.

As was pointed out previously in the Nielsen method, there are two ways of obtaining the solution, one in which a distribution function is found first and then velocities and pressures, and a second shorter method which can be used if pressures are wanted only on the surface of the circular body. In the shorter method the pressure on the body is obtained directly from the boundary conditions by one integration. The shorter method has two advantages, (1) that only one integration is necessary, and (2) that the integration is much easier to perform since there are no singularities in the integrand as there are when we try to find the distribution function from the M's.

It can be said roughly that the accuracies of the Ferrari and Nielsen methods are about the same if the same interval length along the z' axis is used in both methods (see Fig. 5). The Nielsen method has some advantages, however, which should be pointed out. The first advantage is that it is somewhat easier to vary the grid length in the Nielsen method than it is in the Ferrari, since in the Ferrari method the basic summation formulas change so that when each new distribution function slope is computed each term in the summation has to be watched carefully to see that the correct interval is used. This means that the Ferrari method is harder to set up for routine calculation. A second advantage of the Nielsen method is that asymptotic expressions are available for the W_n functions, so that it is possible to make some general statements about the method without performing the complete calculations, i.e., the values near discontinuities can be determined more easily and also the downstream asymptotic behavior can be determined. In the Nielsen expression for determining the pressure there is also the advantage (from the point of view of analyzing the results) that the pressure splits into two parts, one being the local (Ackeret) value and a second part being the effect of all the upstream influence. Ferrari, on the other hand, is able to solve the problem in which the radius

of the body varies along its axis, although this problem is more difficult from the computational point of view inasmuch as it is harder to set up in a routine manner.

The actual computational time required for all three methods is approximately the same. The difficulty in using any one of the three methods occurs in setting the problem up for computation. The Nielsen-Matteson method is the simplest to set up if the various tables of influence coefficients are available. The Ferrari method is not too difficult to prepare for computation. However, some of the computations involved are long and require a good deal of concentration. As far as the Nielsen method is concerned, there is no great difficulty either in applying the method to a specific problem or in carrying out the computations as long as the W_n functions are available.

VI. DISCUSSION OF RESULTS

In the calculations for the various theories a basic Mach number of $M = \sqrt{2}$ was taken, since this simplifies the computation and since the velocity data can later be converted to any desired Mach number by the usual Prandtl-Glauert transformation. In addition, the velocities were nondimensionalized with respect to the uniform cross-flow velocity induced by the shock wave, so that in order to get the results for a shock wave of some particular strength, it is necessary to multiply the nondimensional ratios by the cross-flow velocity.

In the Nielsen method the convolution integrals were evaluated numerically using Simpson's rule with intervals of $z' = 0.2$, whereas the Ferrari curves were obtained by the approximations described before with the interval $z' = 0.5$. Some computations were done with $\Delta z' = 0.25$, and these seem to indicate that the rougher steps give a good approximation at least for the lower-order singularities. A comparison of the curves shows that the methods compare quite well for both ϕ_n and $\partial\phi_n/\partial z'$ at least up to $n = 3$: see Fig. 5.

The first point at which all three theories can be compared is in the values of the perturbation velocities u' and v'_θ. Since the Nielsen and Ferrari theories compare well on the basis of their Fourier components, ϕ_n and $\partial\phi_n/\partial z$, they will of course still have a good comparison when the components are added up. Fig. 6 is a plot of the axial and tangential perturbation velocities vs z' for different meridional angles as given by the three different theories. The heavy lines that are drawn in are faired curves based on points from all the theories and also a knowledge of the endpoints

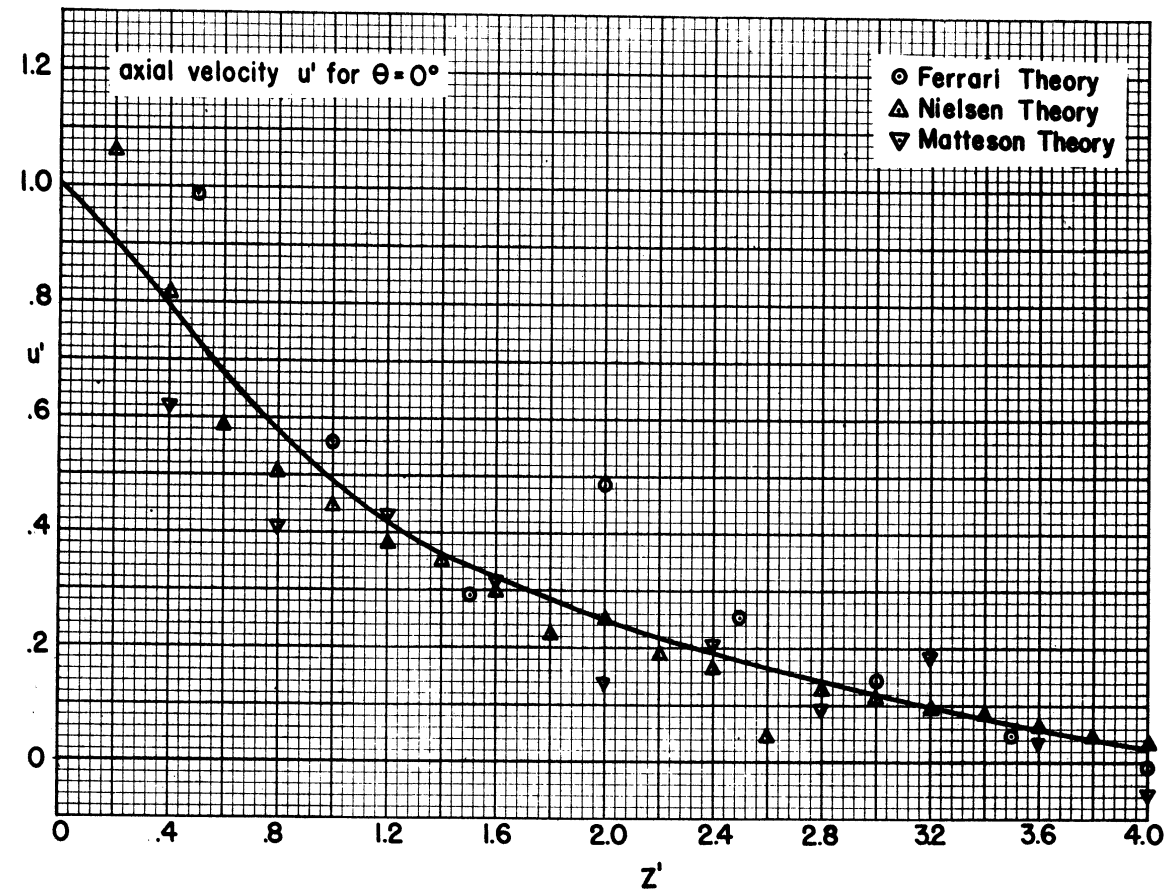

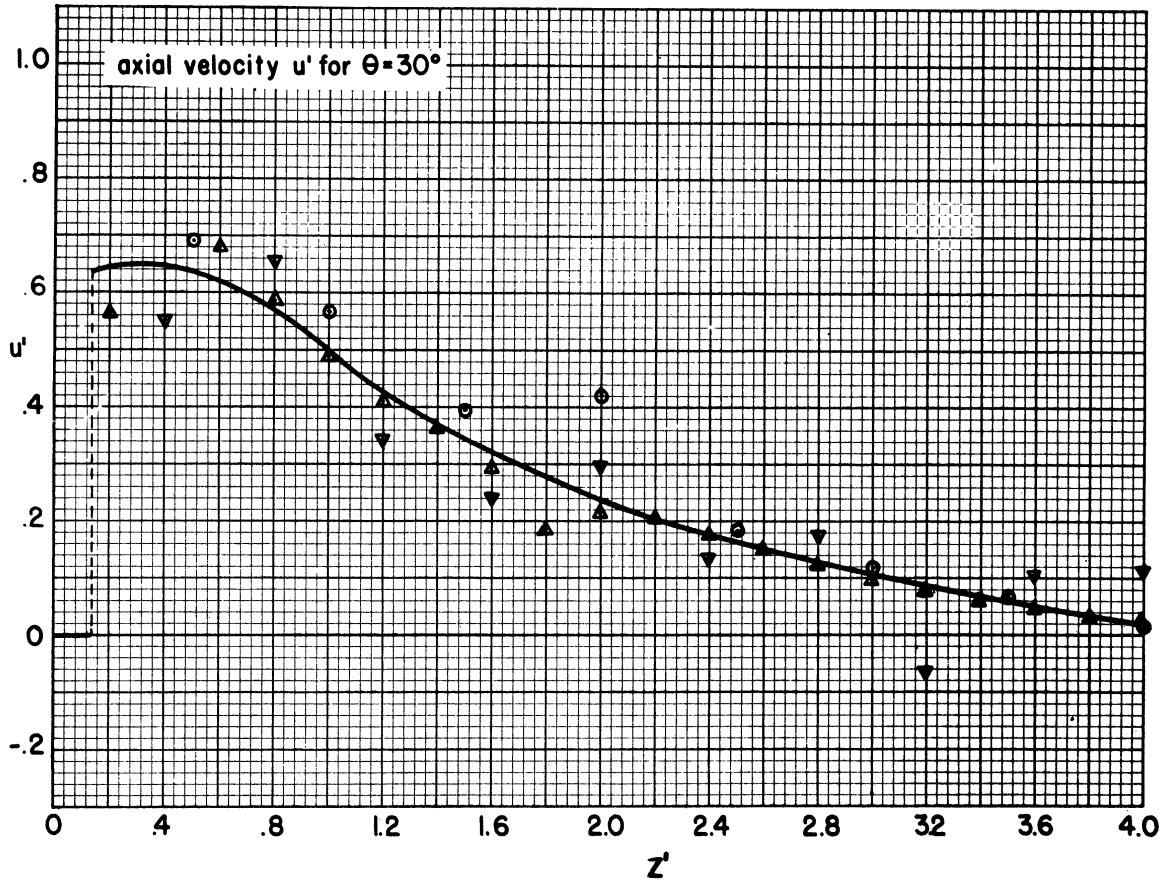

Fig. 6 Nondimensionalized velocities induced on a cylinder by a linearized shock wave. $M=\sqrt{2}$

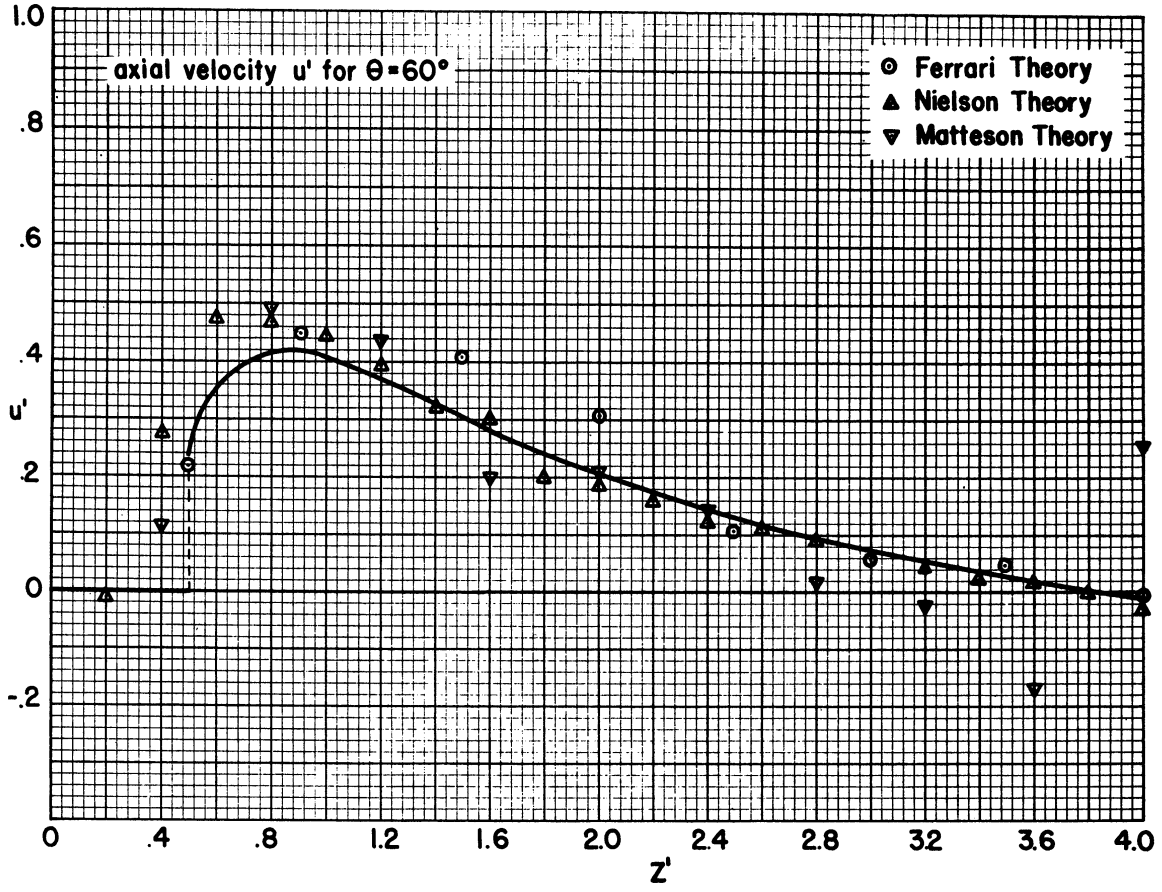
axial velocity u' for Θ=60°
Ferrari Theory
Nielson Theory
Matteson Theory
1.0
.8
.6
.4
.2
0
-.2
u'
0
.4
.8
1.2
1.6
2.0
2.4
2.8
3.2
3.6
4.0
Z'

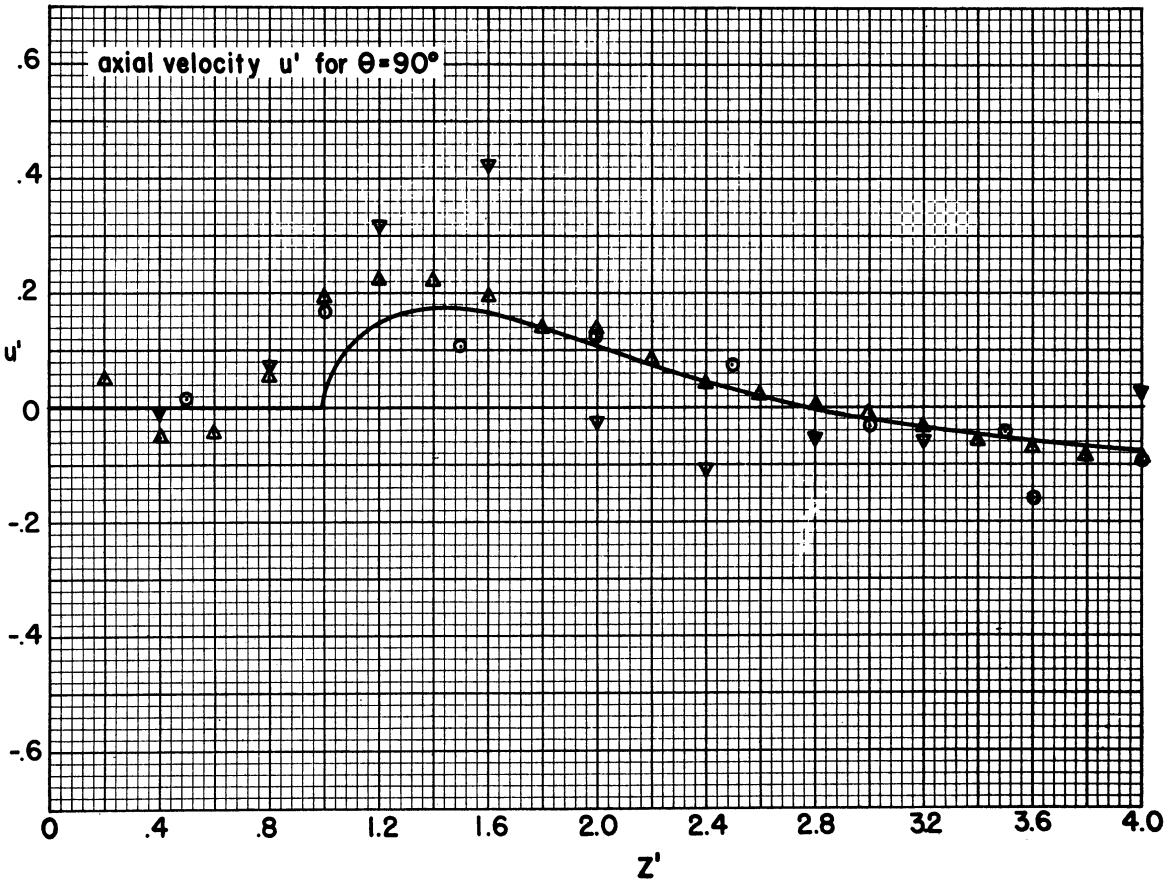
axial velocity u' for Θ=90°
.6
.4
.2
0
-.2
-.4
-.6
u'
0
.4
.8
1.2
1.6
2.0
2.4
2.8
3.2
3.6
4.0
Z'

Fig. 6 (cont.)

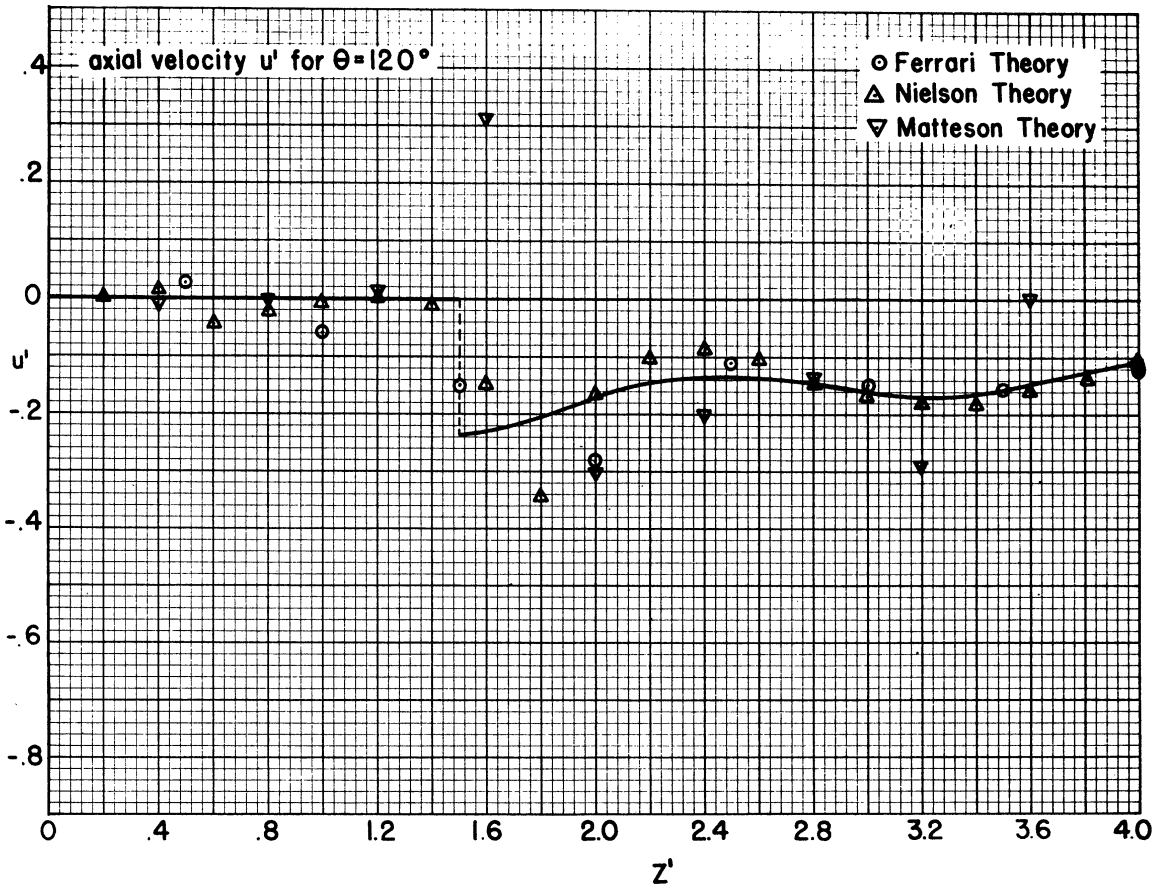
axial velocity u' for Θ=120°
Ferrari Theory
Nielson Theory
Matteson Theory
.4
.2
0
-.2
-.4
-.6
-.8
u'
0
.4
.8
1.2
1.6
2.0
2.4
2.8
3.2
3.6
4.0
Z'

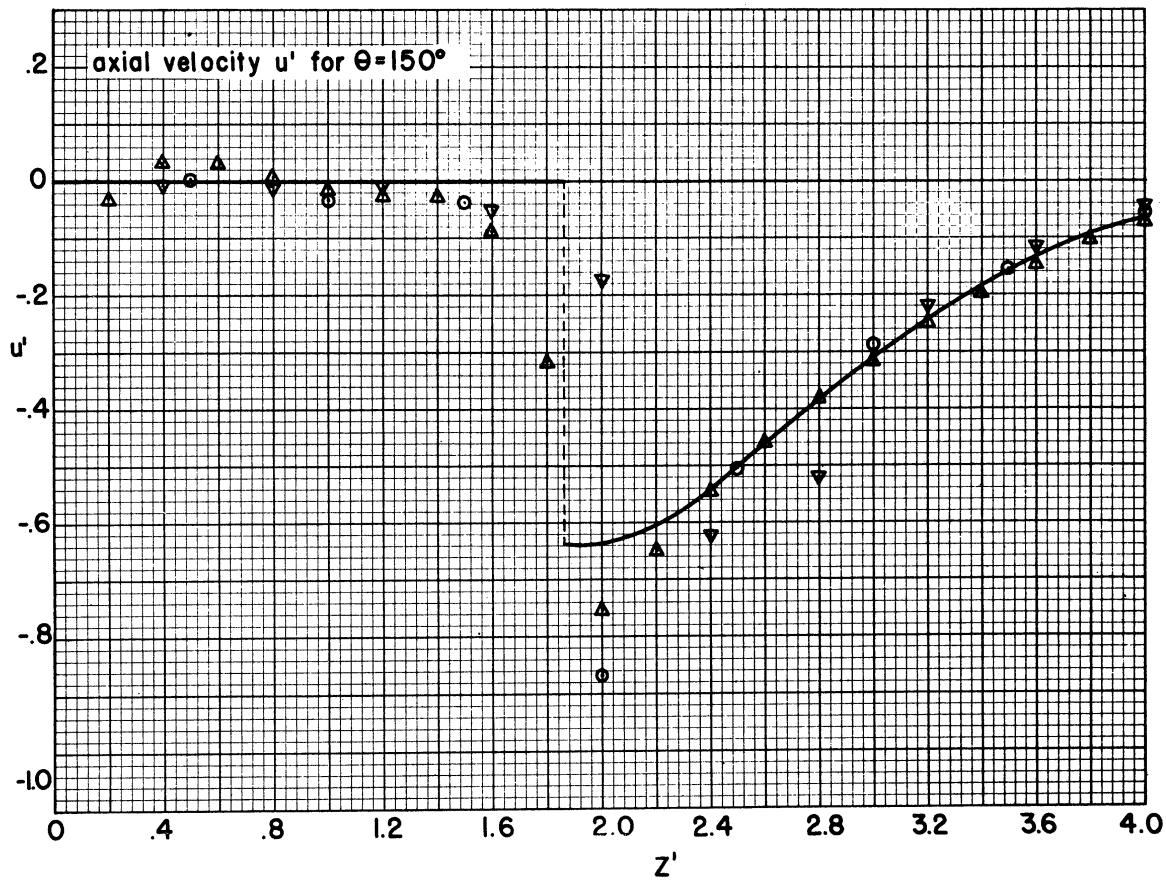
axial velocity u' for Θ=150°
.2
0
-.2
-.4
-.6
-.8
-1.0
u'
0
.4
.8
1.2
1.6
2.0
2.4
2.8
3.2
3.6
4.0
Z'

Fig.6 (cont.)

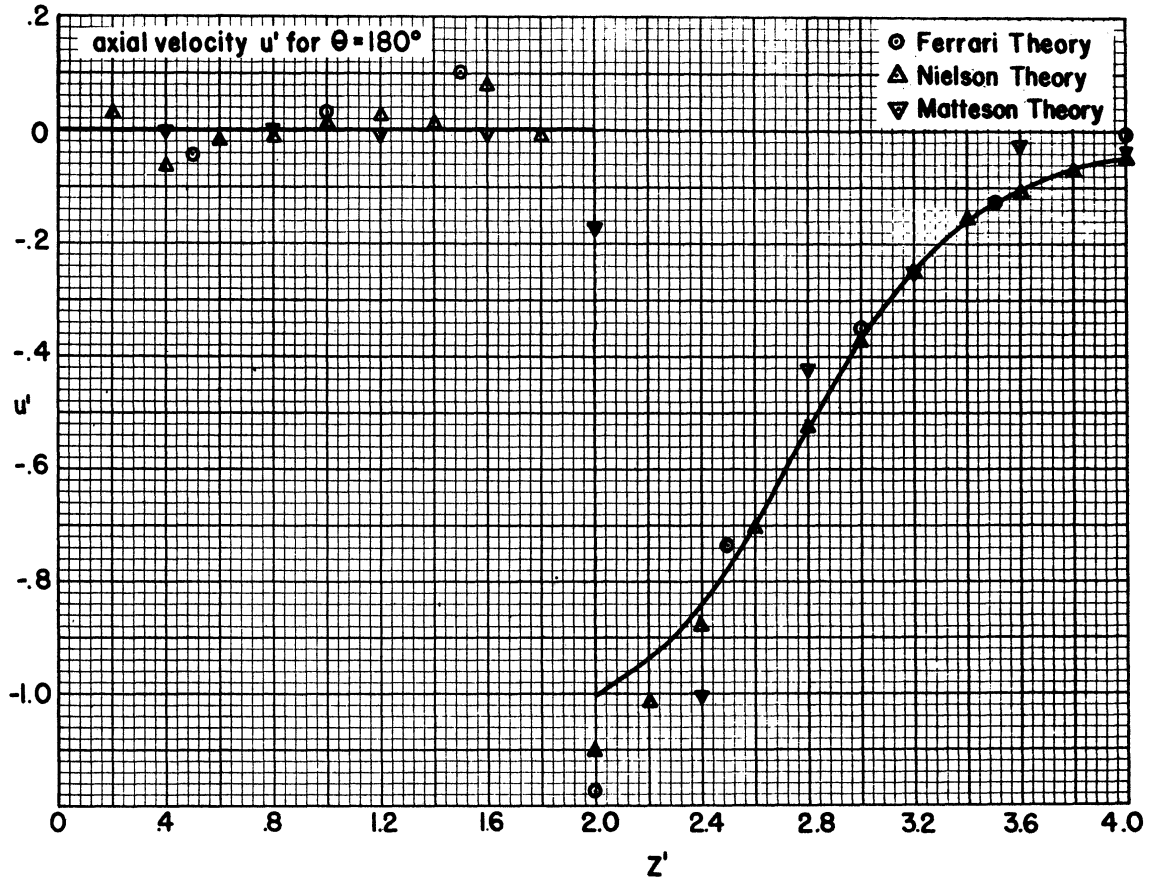
axial velocity u' for Θ=180°
Ferrari Theory
Nielson Theory
Matteson Theory
.2
0
-.2
-.4
u'
-.6
-.8
-1.0
0
.4
.8
1.2
1.6
2.0
2.4
2.8
3.2
3.6
4.0
Z'

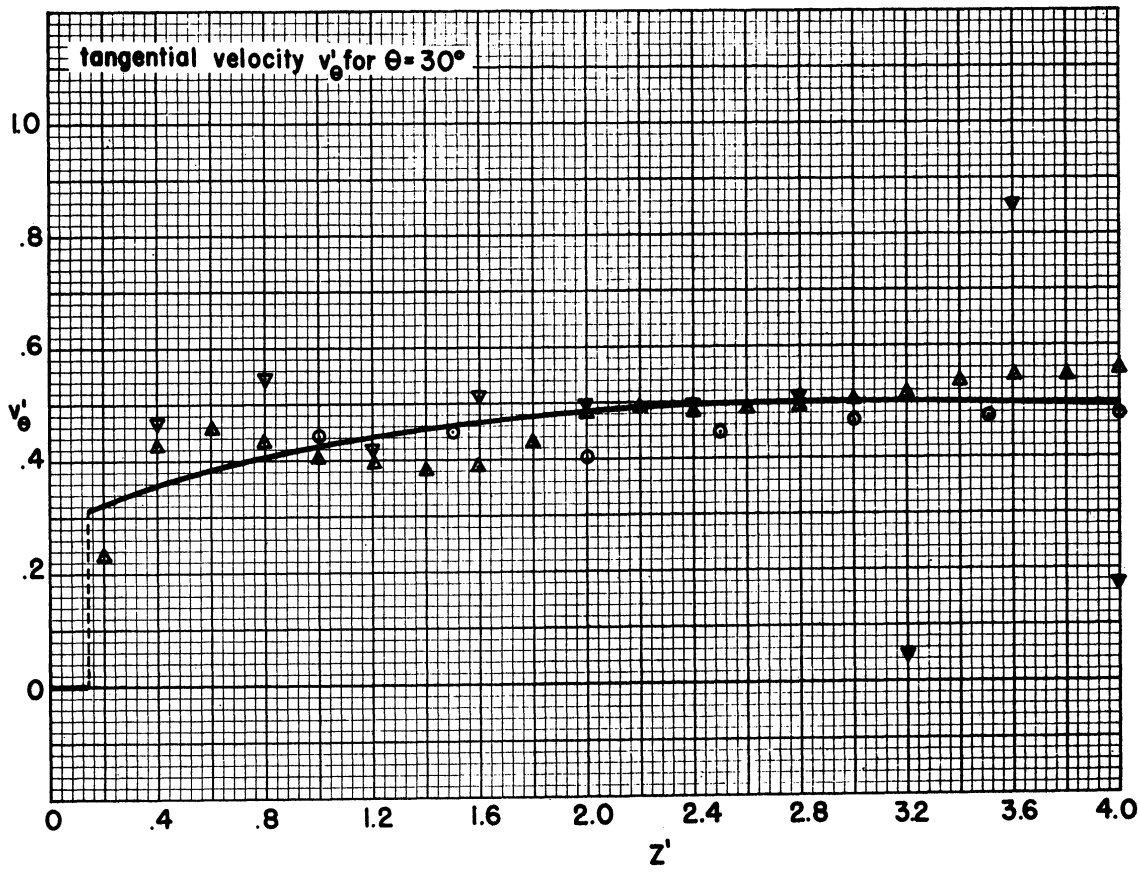
tangential velocity v'θ for Θ=30°
1.0
.8
.6
v'θ
.4
.2
0
0
.4
.8
1.2
1.6
2.0
2.4
2.8
3.2
3.6
4.0
Z'

Fig. 6(cont.)

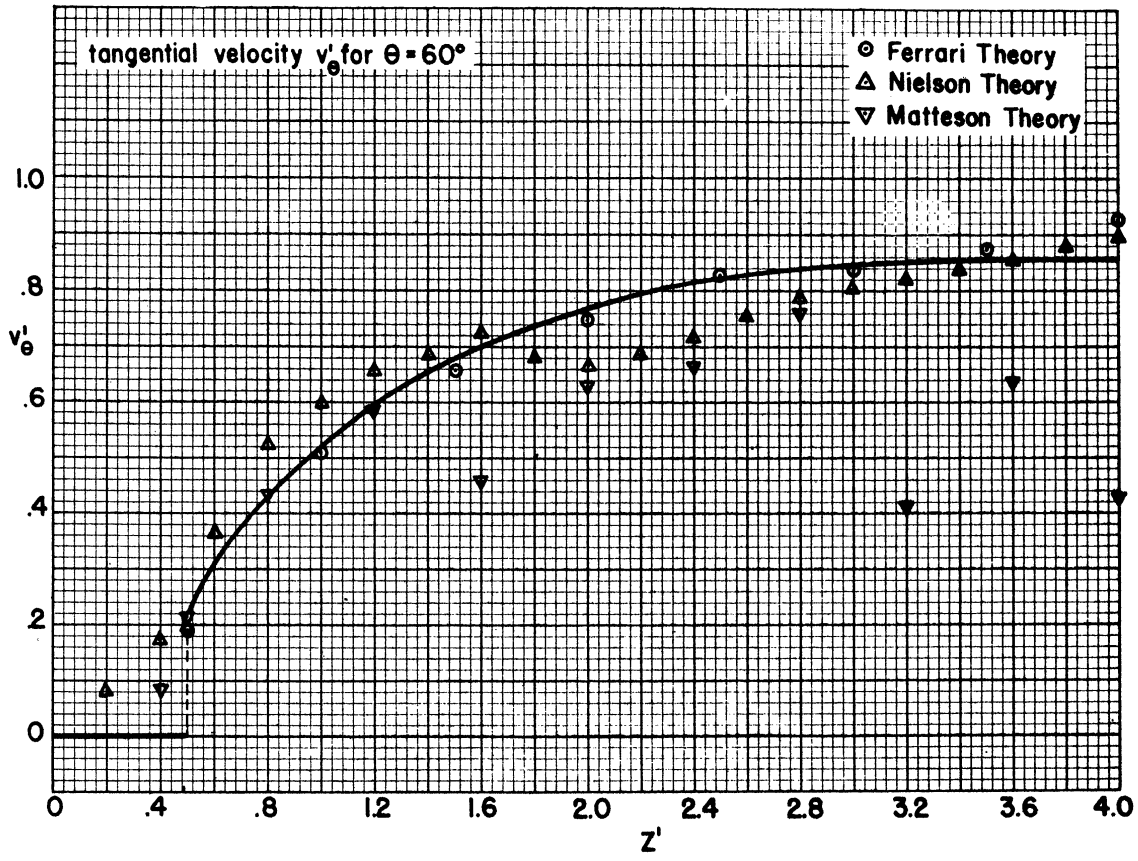
tangential velocity v'_θ for $\theta = 60°$
Ferrari Theory
Nielson Theory
Matteson Theory
1.0
.8
v'_θ
.6
.4
.2
0
0
.4
.8
1.2
1.6
2.0
2.4
2.8
3.2
3.6
4.0
Z'

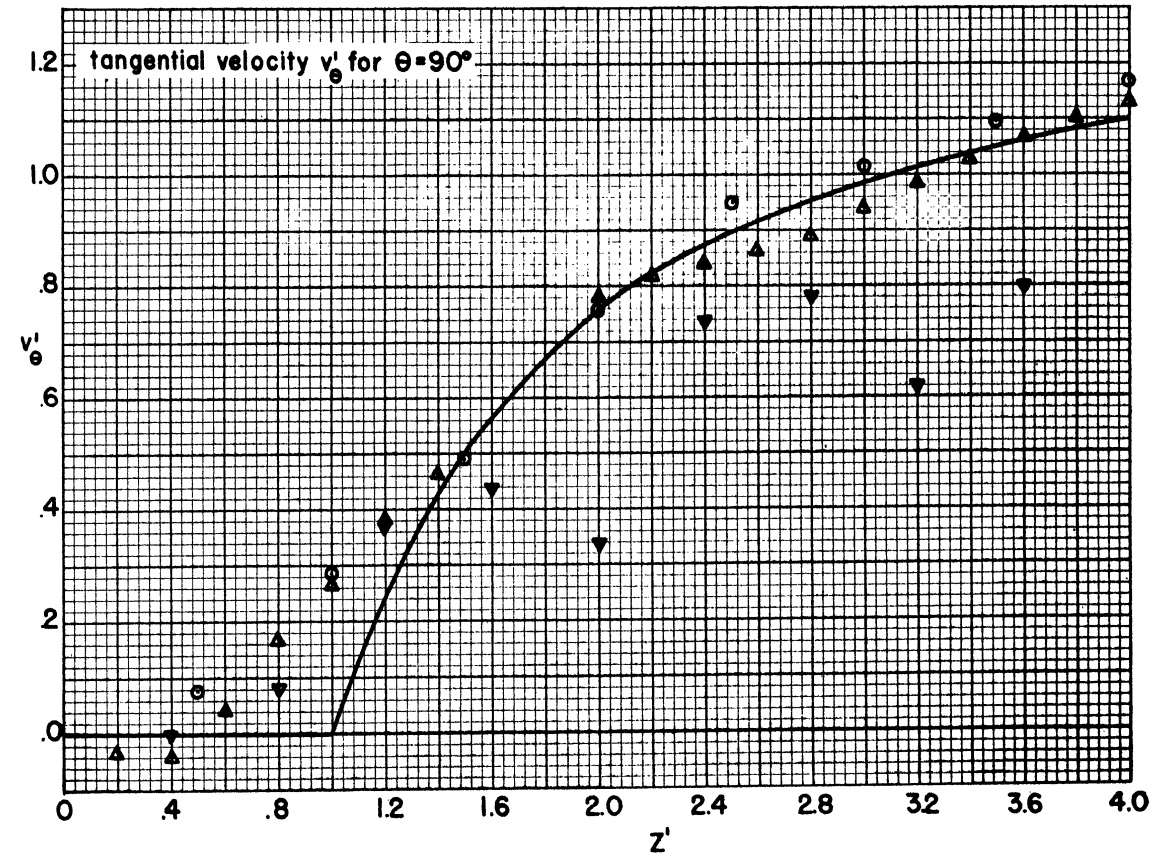
tangential velocity v'_θ for $\theta = 90°$
1.2
1.0
.8
v'_θ
.6
.4
.2
.0
0
.4
.8
1.2
1.6
2.0
2.4
2.8
3.2
3.6
4.0
Z'

Fig. 6 (cont.)

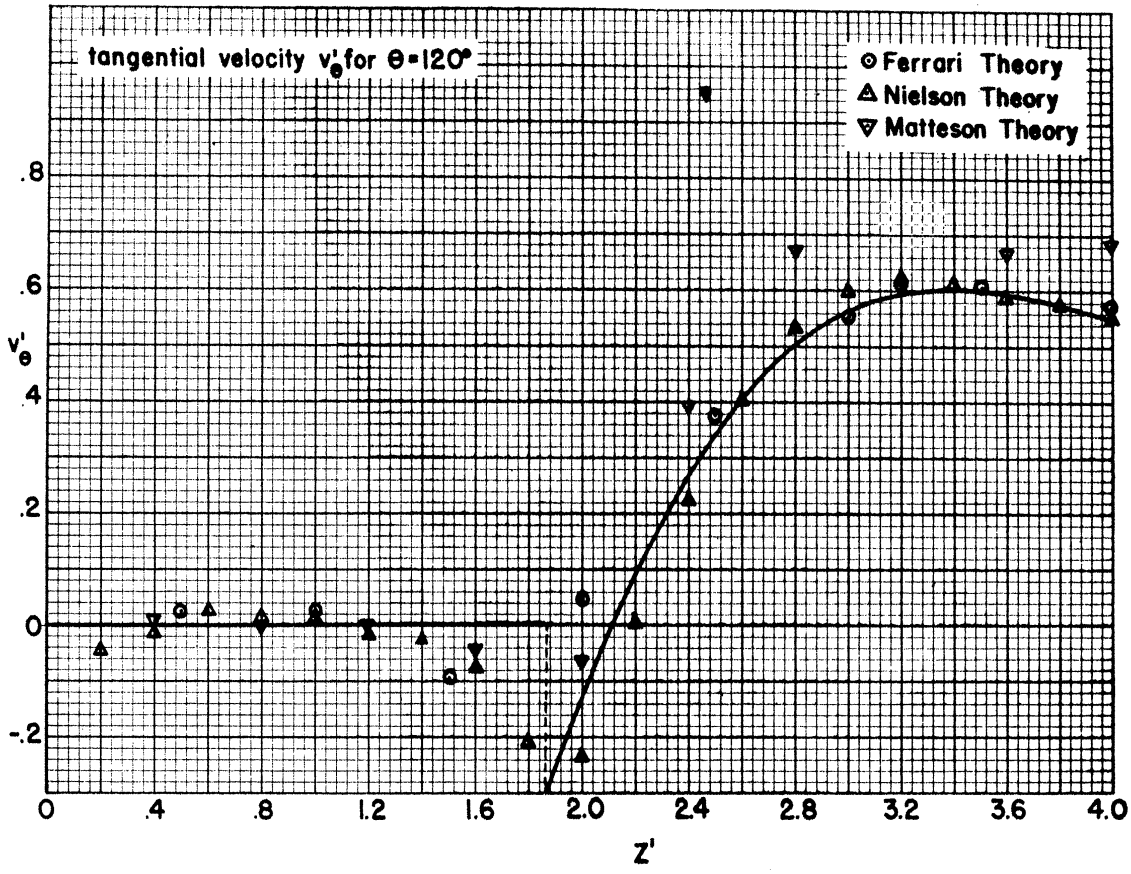

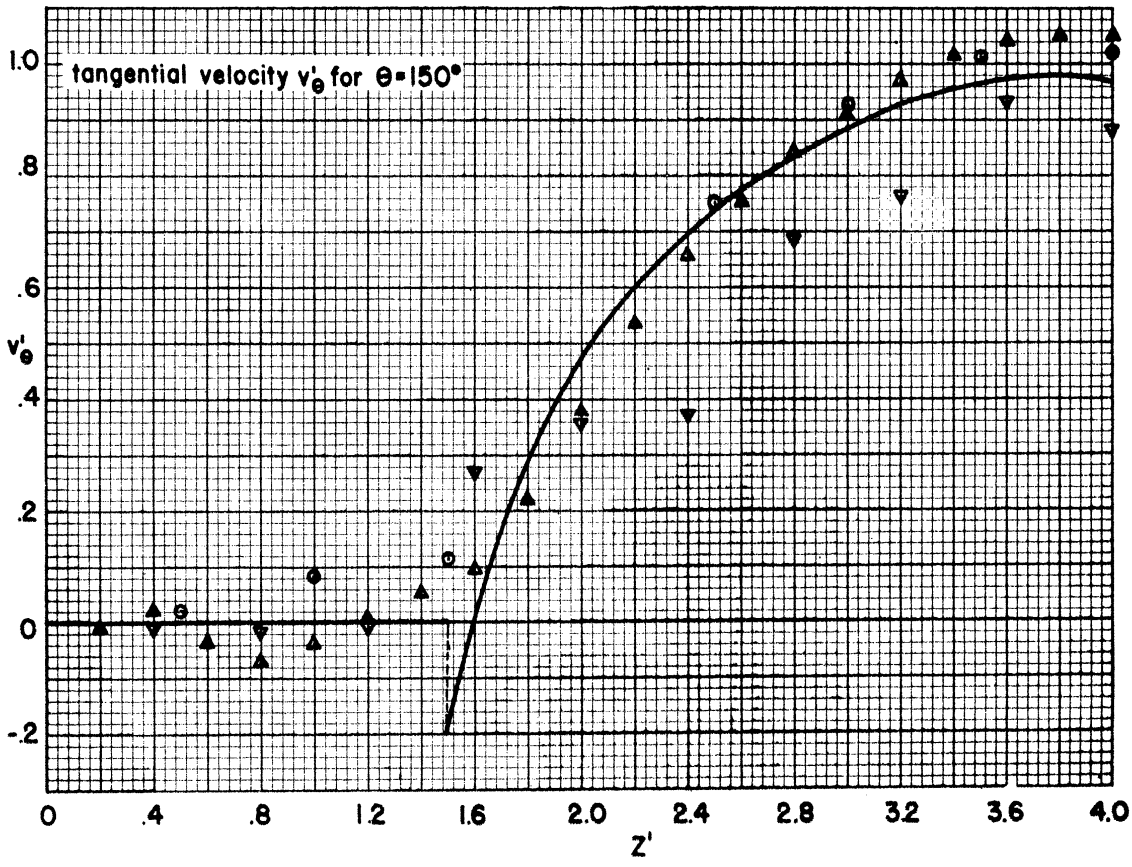

Fig. 6(concluded).

of the curves. It can be observed that both the Nielsen and Ferrari points have a variation from the faired curve and that the two theories do not depart in exactly the same way, which means that there is some variation due both to the approximation and to the finiteness of the number of terms in the Fourier series. Near the discontinuities there is a softening of the effects, as would be expected from the relatively small number of terms used in the approximation. Since there are no exact solutions without some approximation, there is no absolute criterion for the error in the solution; the only comparison that can be made is between the faired heavy curve and the points given by theory.

The pressure was computed next from the velocity components by converting them to $M = 1.87$ (the Mach number of tests in Ref. 8) and by selecting a cross-flow velocity corresponding to $\delta = 11.2°$ and $4.0°$. For a comparison, the pressure was calculated both from the exact isentropic relation which involves both velocity components, i.e., u' and v'_θ on the surface, and from the linearized expression in which the pressure depends only on the axial velocity u'. From the linearized pressure relation we would conclude that the asymptotic pressure on the cylinder due to the cross-flow would be independent of θ, whereas there would actually be a nonconstant pressure around the surface due to the asymptotic doublet flow. If the isentropic pressure relation is used, then the effect of the doublet will be included. Also note that the linearized pressure relation implies that all the pressure distributions with δ or M varying will be similar to each other, so that an affine transformation of one or both of the axes is all that is necessary to bring the curves into coincidence. When we include the quadratic terms in the exact expression for the pressure, however, the curves will no longer be exactly similar and the correct (according to the incompressible cross-flow theory) asymptotic pressures will be obtained. Fig. 7 shows the computed results of the exact isentropic pressure ratio and the linearized pressure ratio, and the experimental results of Ref. 8 for shock deflection angles of $\delta = 11.2°$ and $\delta = 4.0°$. Fig. 8 gives a composite picture of the theoretical pressure distribution. In the $\delta = 11.2°$ case we see that there is considerably more percentage error between the exact and linearized pressure ratio than in the case $\delta = 4.0°$. In general, the divergence between the linearized and exact expressions for the pressure is more serious at points downstream of the intersection, than at the intersection, due to the fact that the axial velocity steadily dies to zero, while the tangential velocities do not.

The comparison between theory and experiment is fairly good, bearing in mind the things pointed out in Ref. 8; that is, there is considerable boundary-layer cross-flow, which changes the surface pressure both by altering the external flow and by providing a channel through which pressure disturbances can propagate. The boundary-layer accumulation is most serious on the lee side of the body, so that the biggest differences between theory and experiment should be found there.

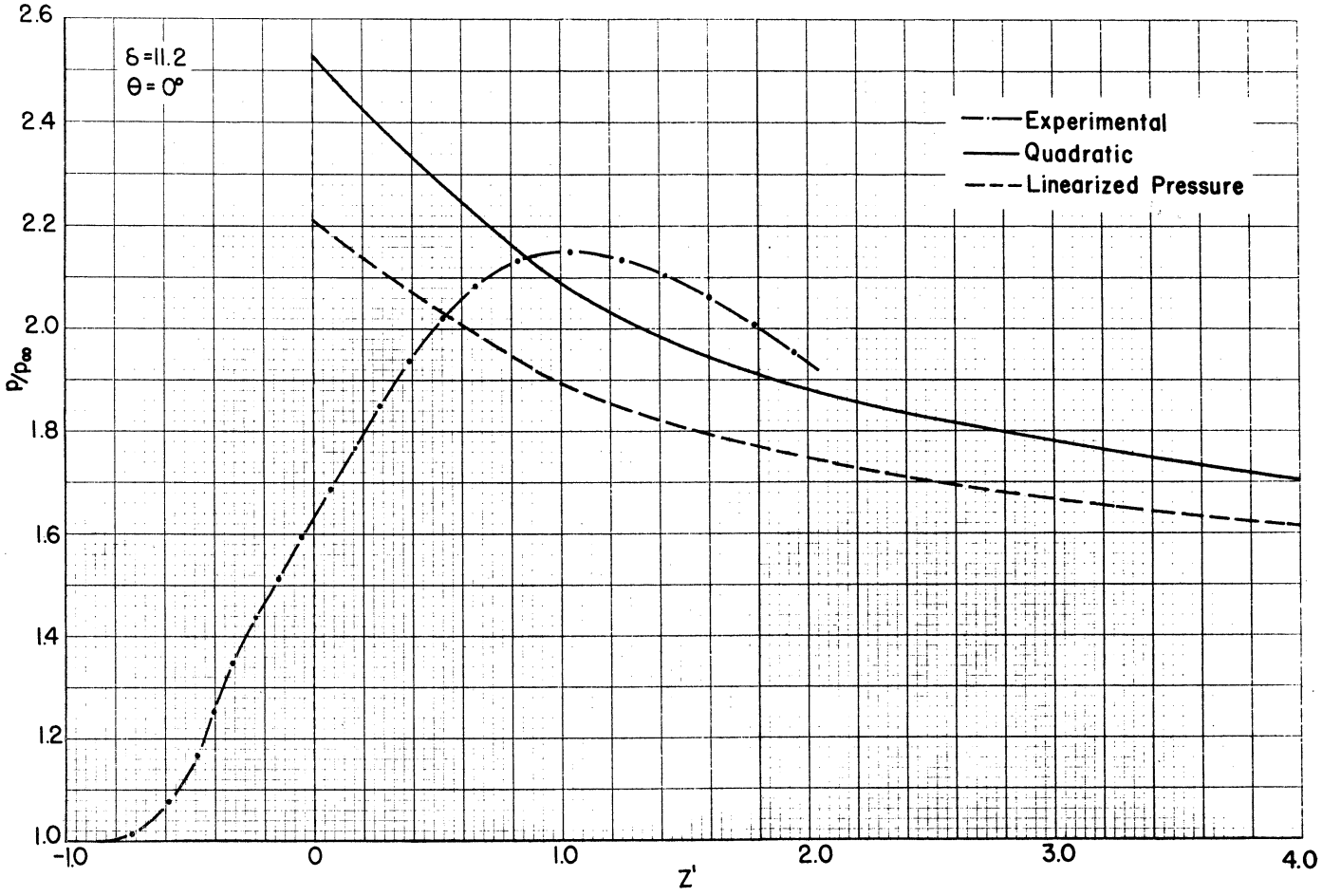

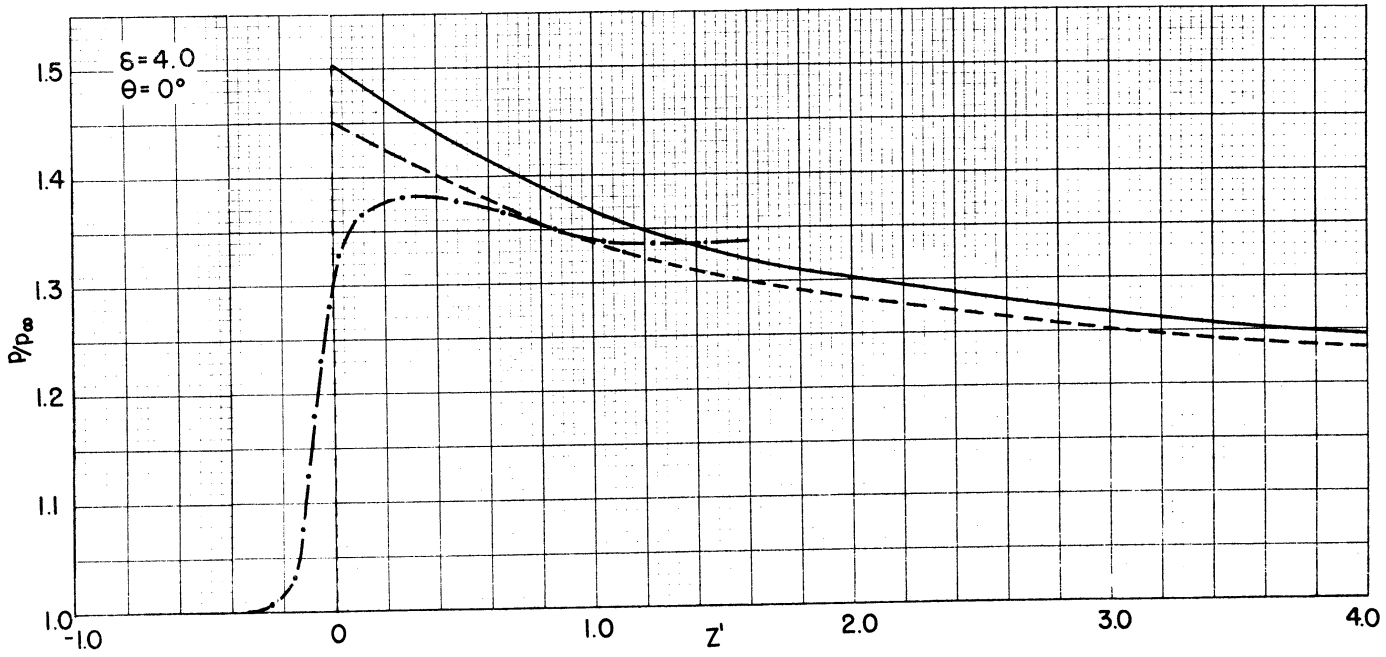

Fig. 7 Pressure Ratio on Cylinder for Shock Deflection δ.

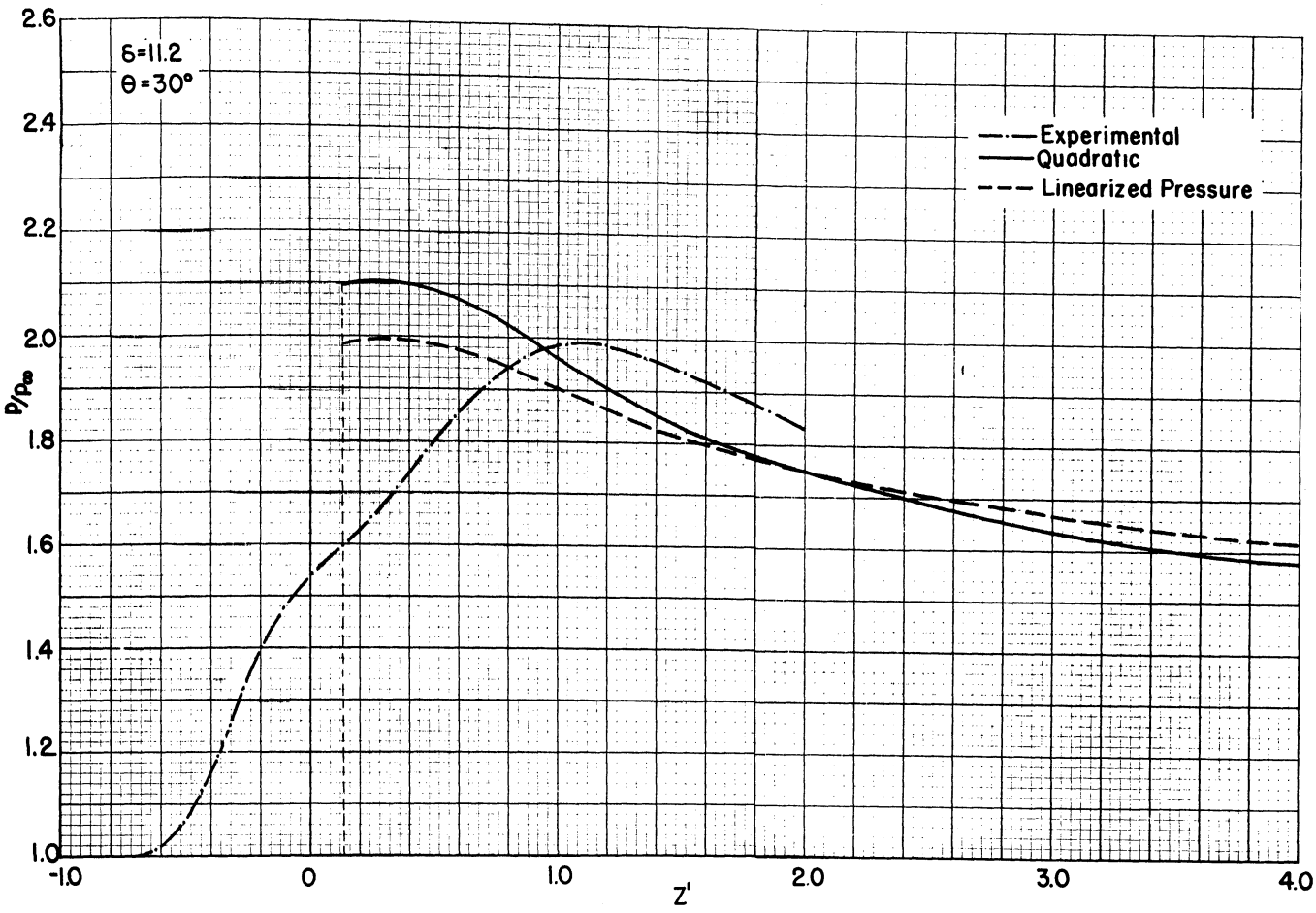
δ=11.2
θ=30°
Experimental
Quadratic
Linearized Pressure
p/p∞
Z'
2.6
2.4
2.2
2.0
1.8
1.6
1.4
1.2
1.0
-1.0
0
1.0
2.0
3.0
4.0

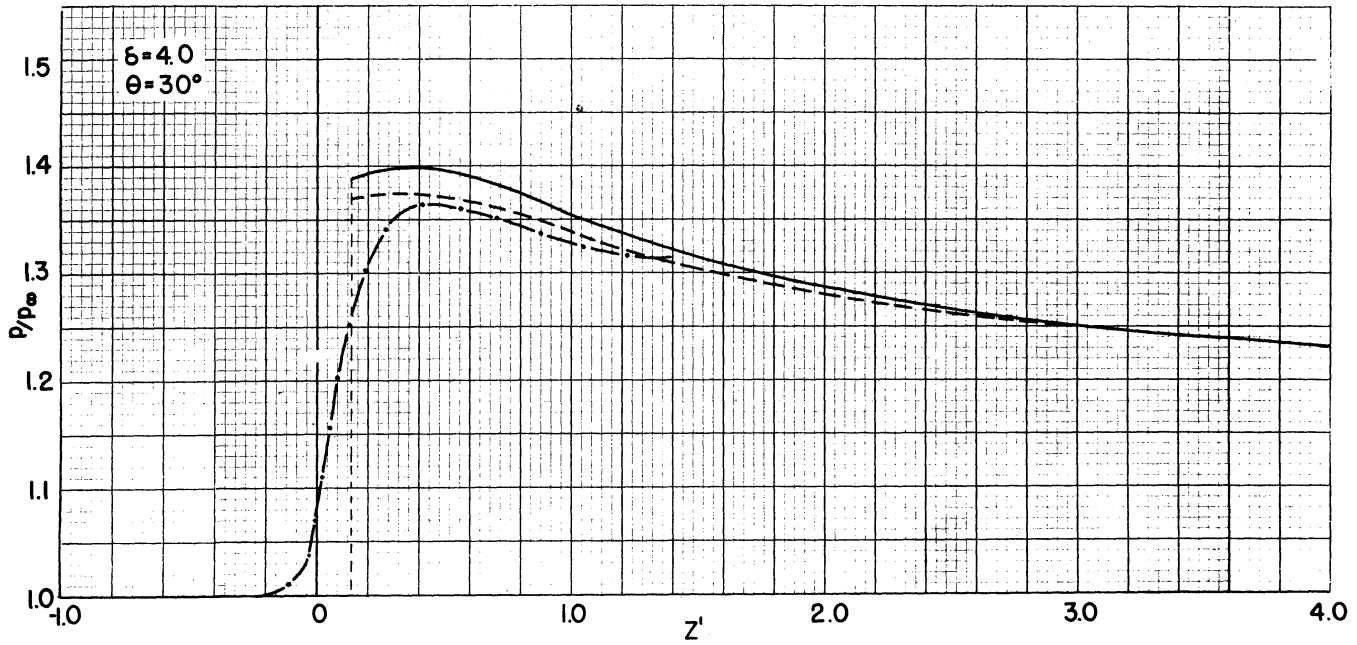
δ=4.0
θ=30°
p/p∞
Z'
1.5
1.4
1.3
1.2
1.1
1.0
-1.0
0
1.0
2.0
3.0
4.0

Fig. 7 (cont.)

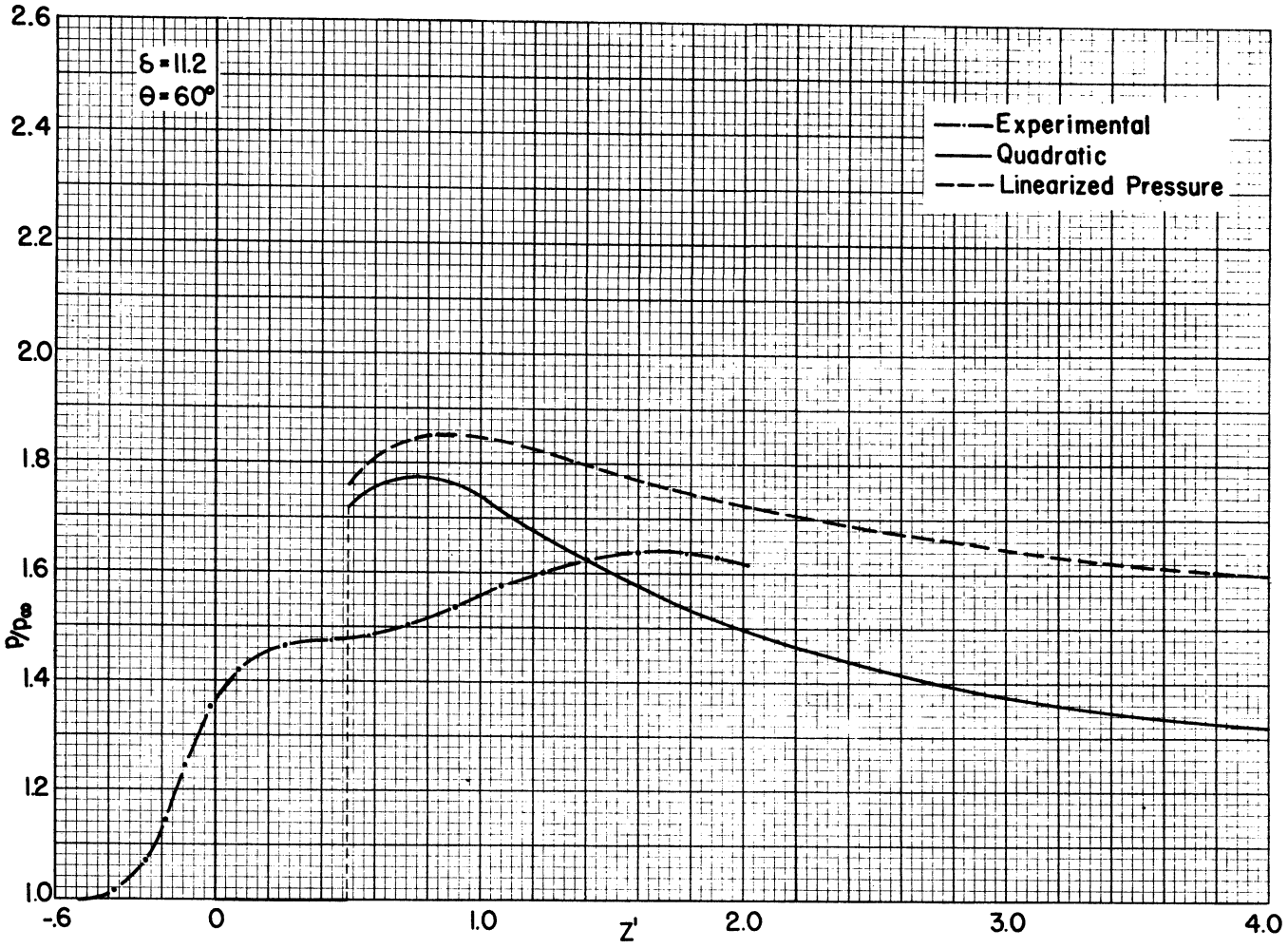
δ=11.2
θ=60°
Experimental
Quadratic
Linearized Pressure
2.6
2.4
2.2
2.0
1.8
1.6
1.4
1.2
1.0
p/p∞
-.6
0
1.0
2.0
3.0
4.0
Z'

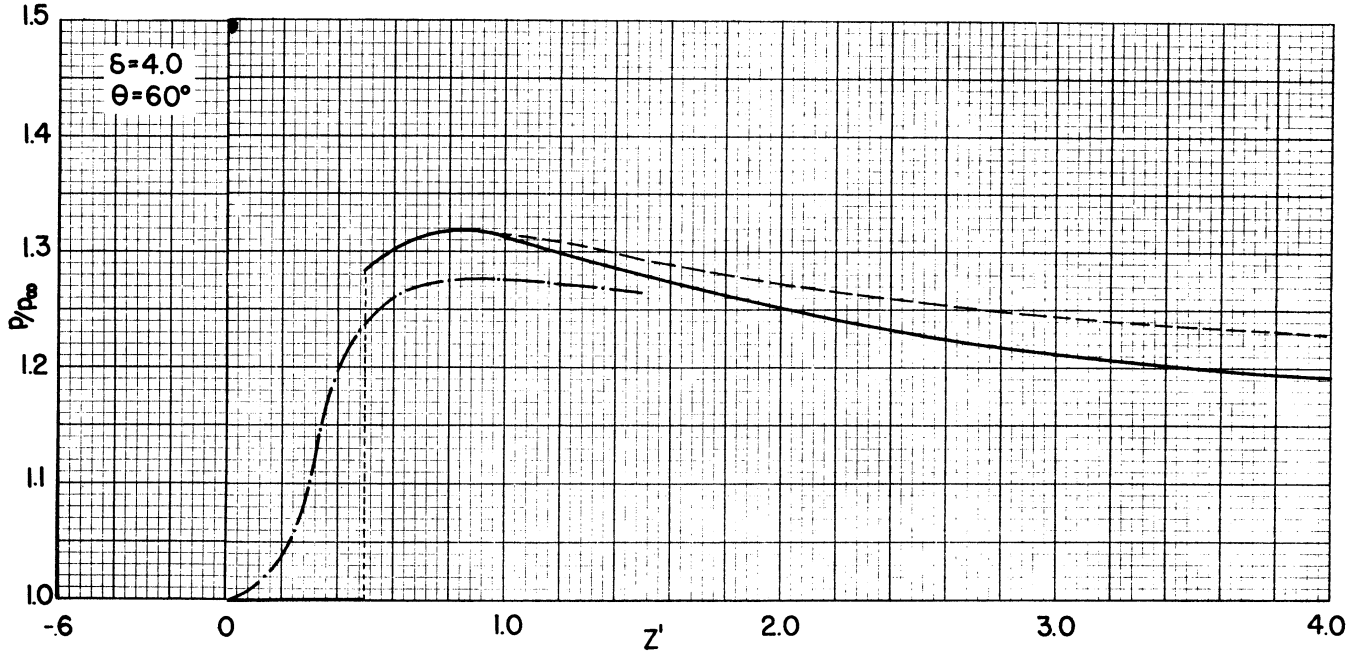
δ=4.0
θ=60°
1.5
1.4
1.3
1.2
1.1
1.0
p/p∞
-.6
0
1.0
2.0
3.0
4.0
Z'

Fig. 7 (cont)

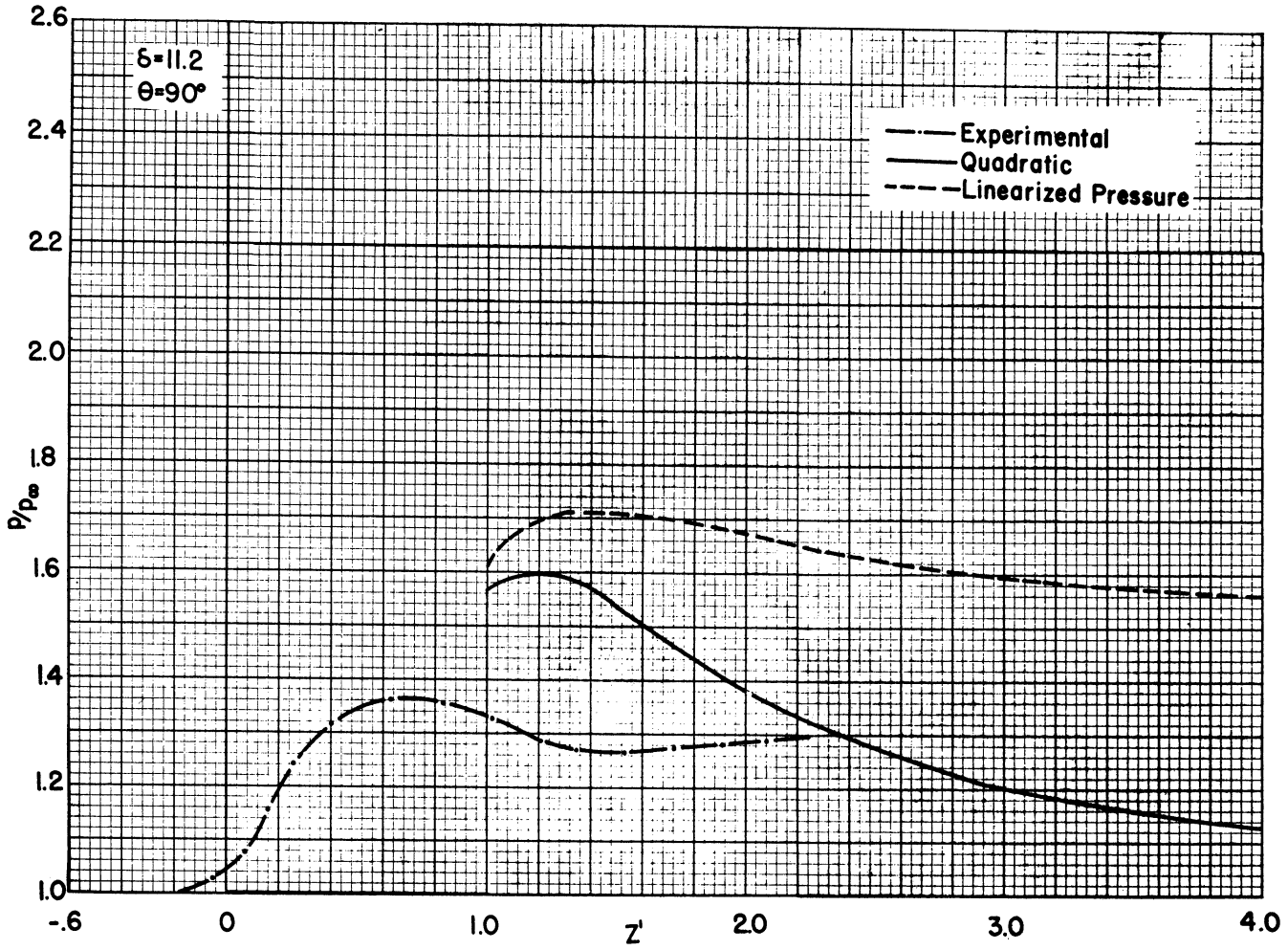
δ=11.2
θ=90°
Experimental
Quadratic
Linearized Pressure
2.6
2.4
2.2
2.0
1.8
1.6
1.4
1.2
1.0
p/p∞
-.6
0
1.0
Z'
2.0
3.0
4.0

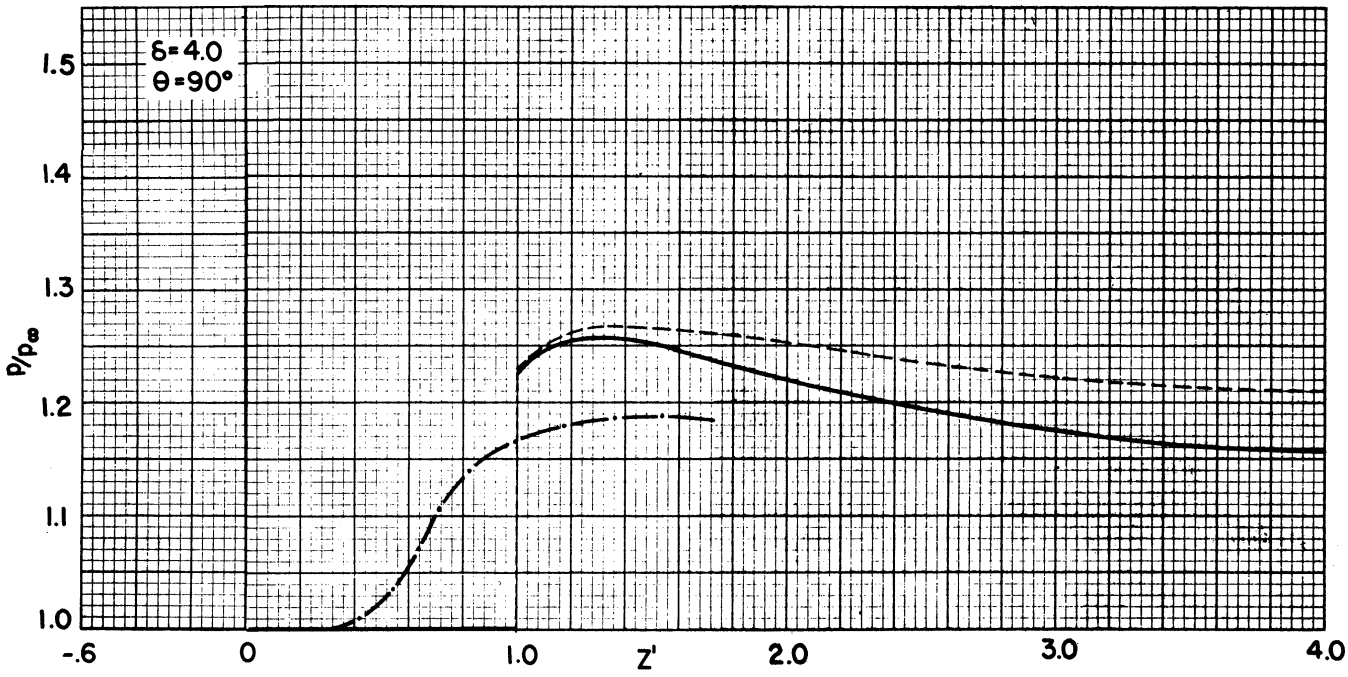
δ=4.0
θ=90°
1.5
1.4
1.3
1.2
1.1
1.0
p/p∞
-.6
0
1.0
Z'
2.0
3.0
4.0

Fig. 7 (cont.)

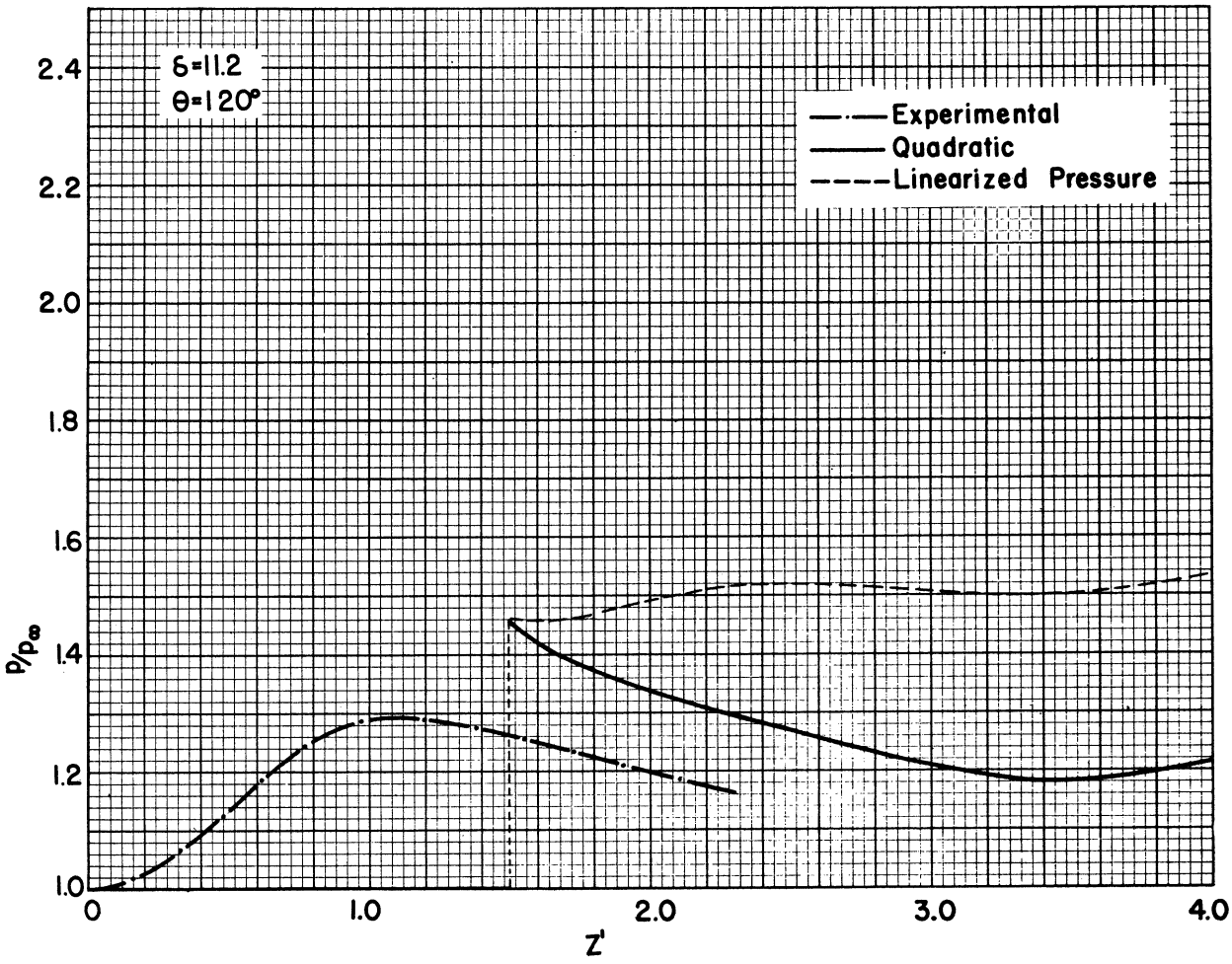
δ=11.2
θ=120°
Experimental
Quadratic
Linearized Pressure
2.4
2.2
2.0
1.8
1.6
1.4
1.2
1.0
p/p∞
0
1.0
2.0
3.0
4.0
Z'

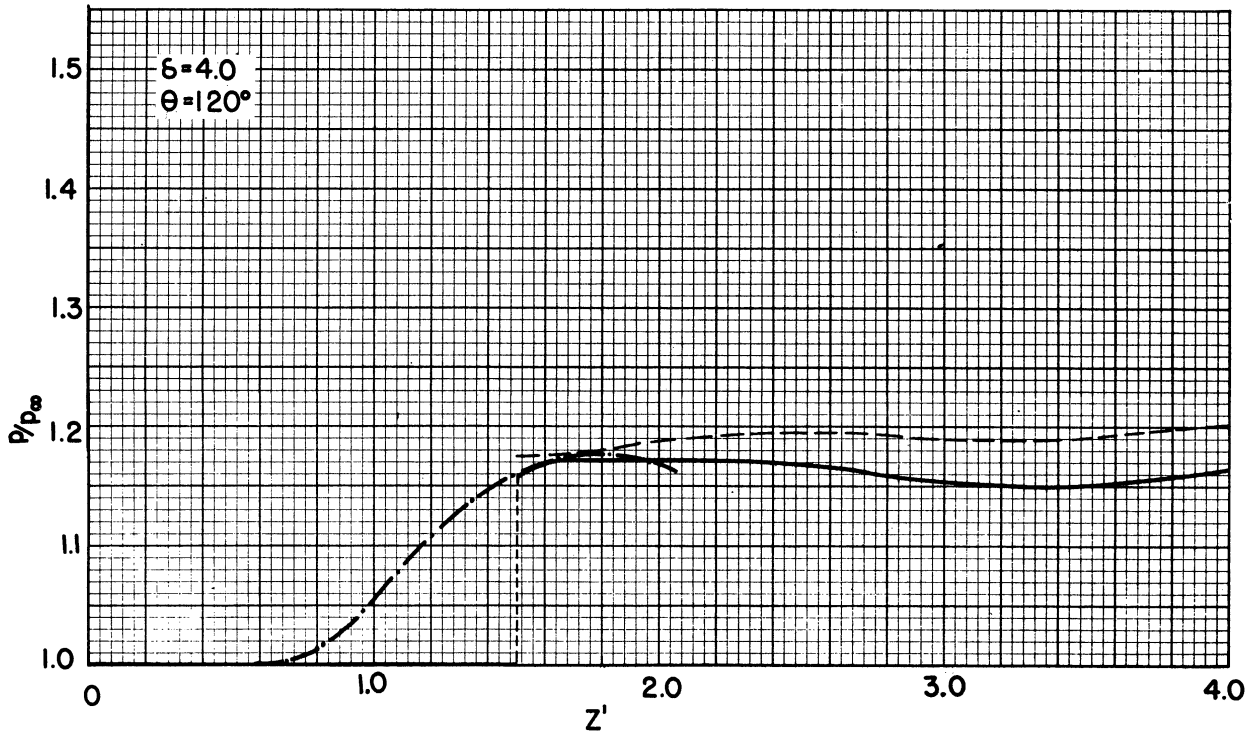
δ=4.0
θ=120°
1.5
1.4
1.3
1.2
1.1
1.0
p/p∞
0
1.0
2.0
3.0
4.0
Z'

Fig. 7(cont.)

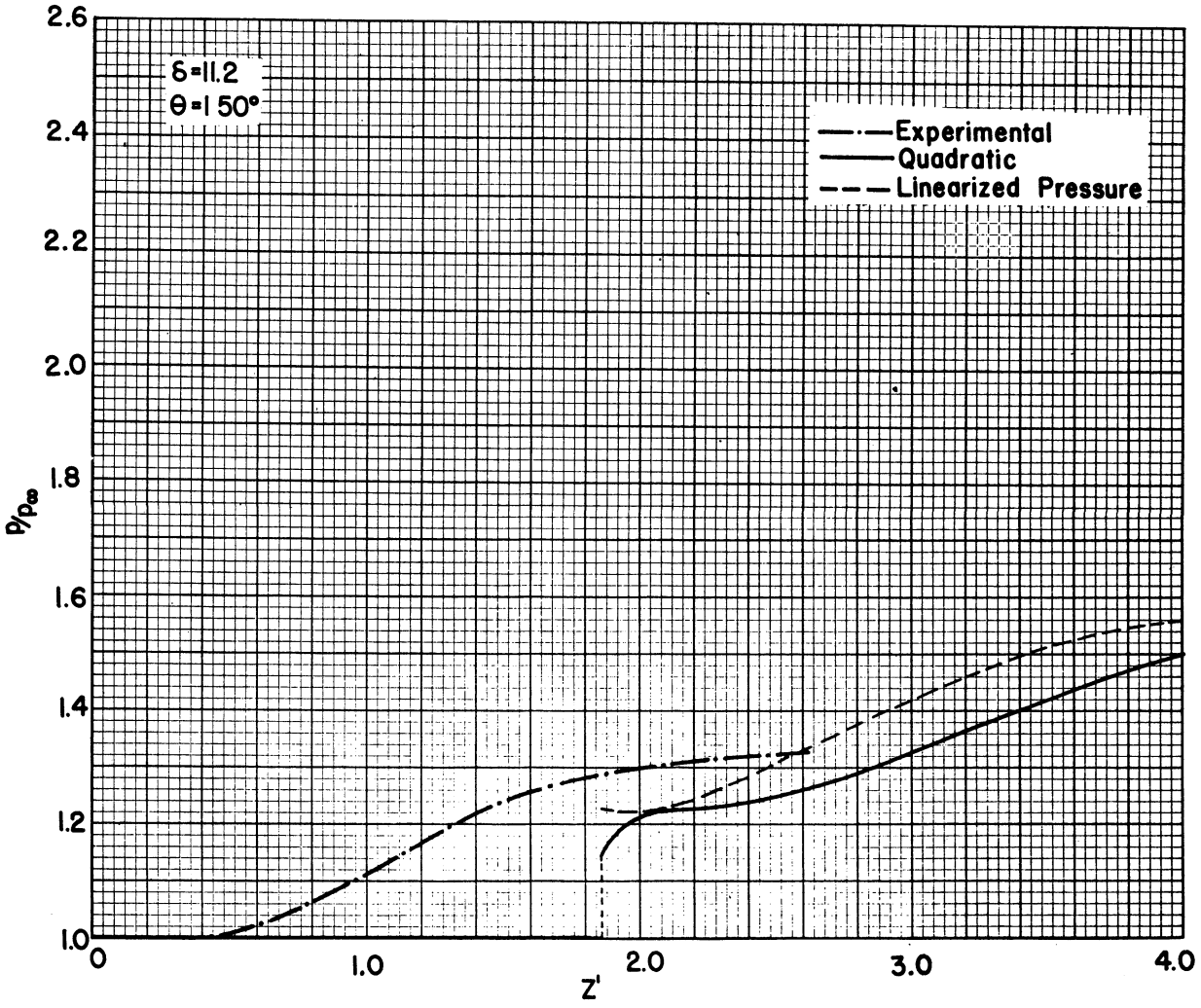
δ=11.2
θ=150°
Experimental
Quadratic
Linearized Pressure
2.6
2.4
2.2
2.0
1.8
1.6
1.4
1.2
1.0
p/p∞
0
1.0
2.0
3.0
4.0
Z'

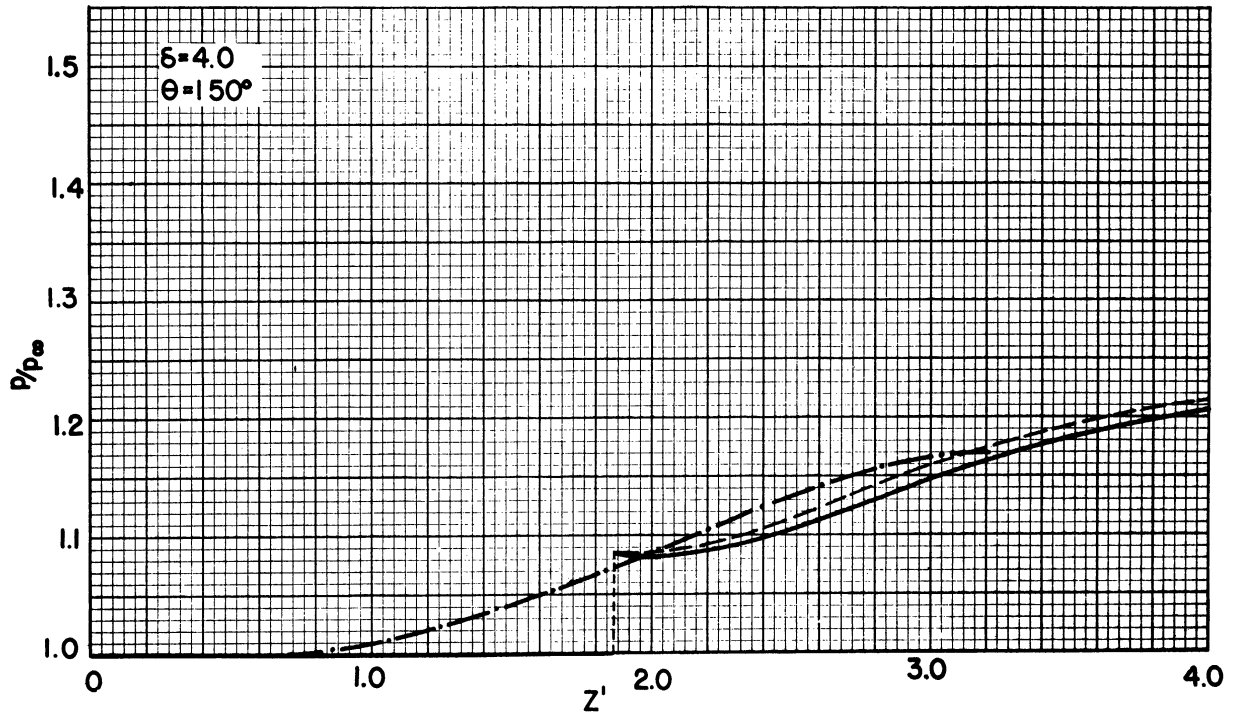
δ=4.0
θ=150°
1.5
1.4
1.3
1.2
1.1
1.0
p/p∞
0
1.0
2.0
3.0
4.0
Z'

Fig. 7 (cont.)

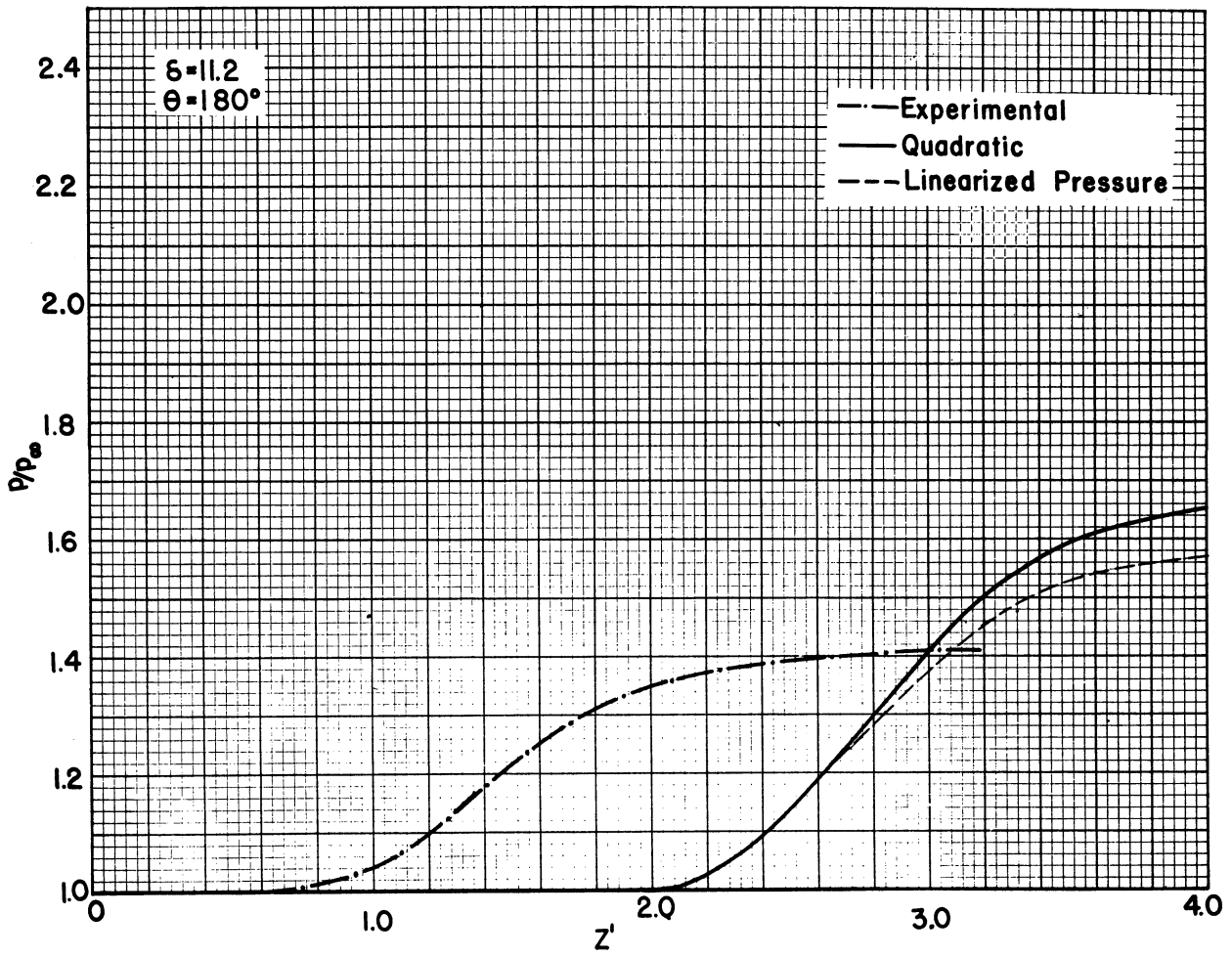

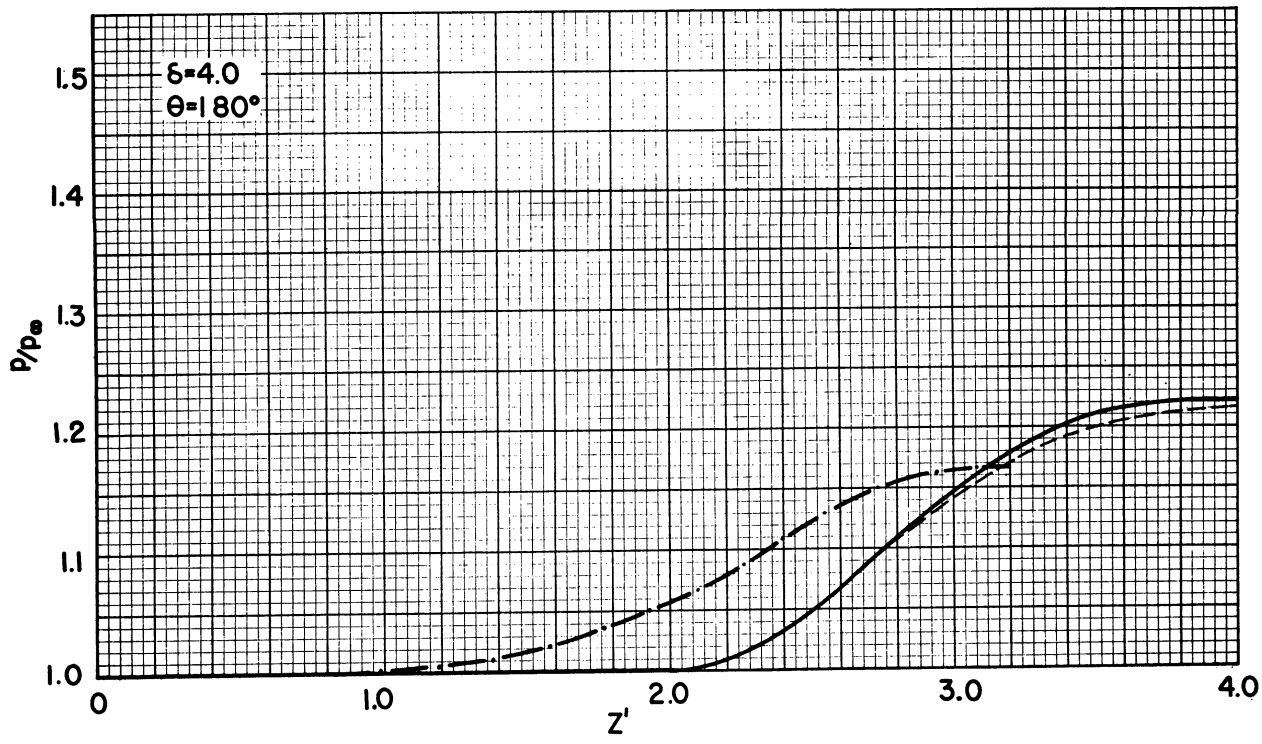

Fig. 7 (concluded)

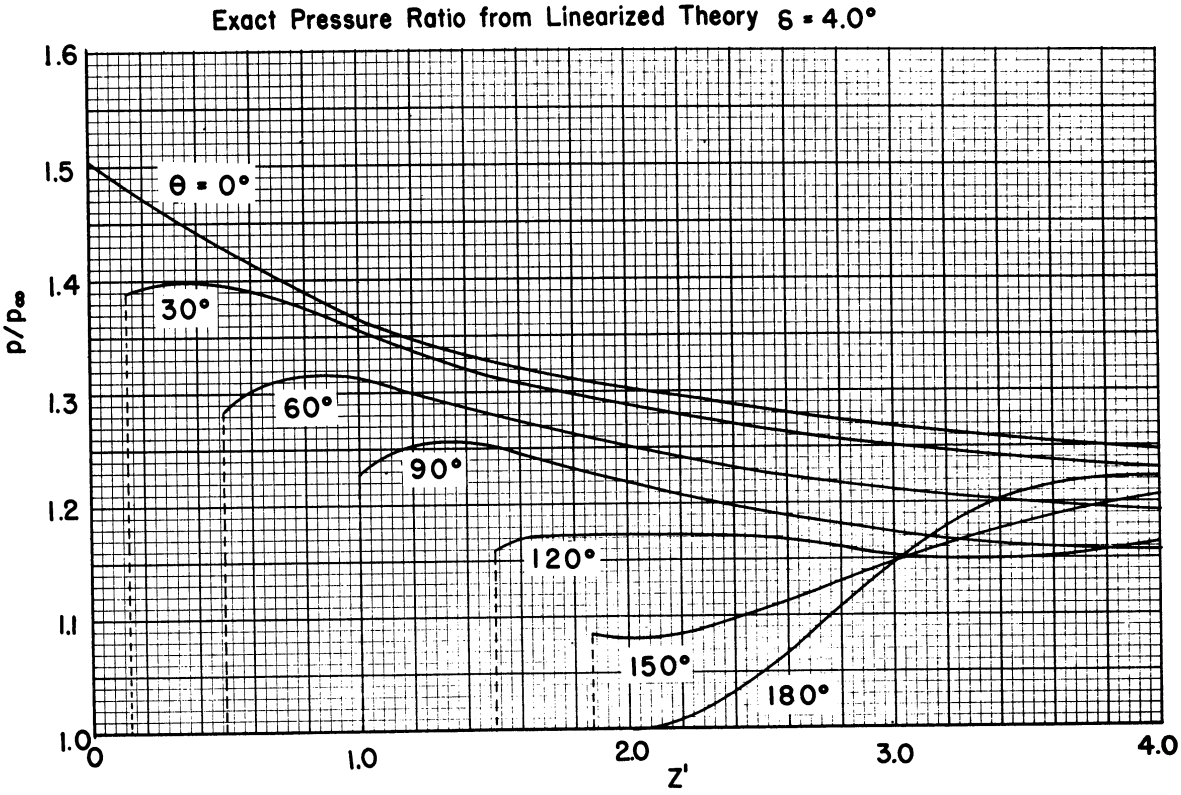

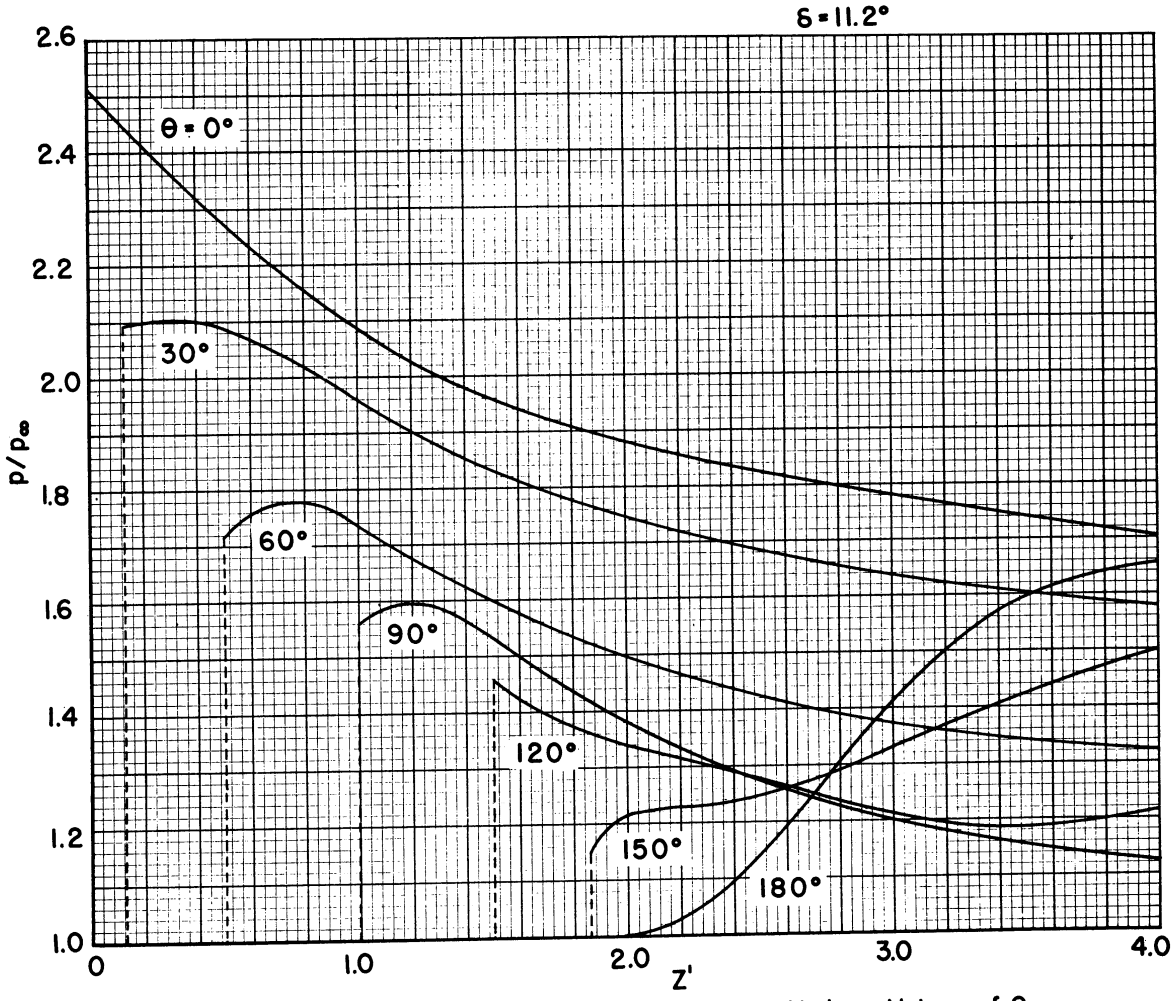

Fig. 8 Composite of Pressure Ratios for Various Values of θ.

In the region near the shock we see that the theory indicates that pressure and velocity both should have very sharp peaks, which are impossible to get from experiment due to the presence of the boundary layer. This explains the difference between the experimental and theoretical curves in Fig. 7 of Ref. 8. It should be noted that the linearized theory does not give an accurate description of the flow near the shock wave, particularly for the higher deflection angles, since the theory assumes that the Mach number is everywhere the free-stream Mach number, and this is of course not a very good assumption near the shock wave. In fact, the linear theory predicts a "shock jump" in the pressure ratio of 1.44 for $\delta = 4°$ and 2.20 for $\delta = 11.2°$, while the values computed from shock tables (Ref. 14) are 1.51 and 3.26. It is possible that the experimental and the theoretical curves are not for exactly the same flow conditions, although they were made to coincide as nearly as possible.

Since the shock angle and the Mach angle are not the same, the "intersection distance" in the actual case was taken to be the axial distance between the point where the shock plane first hits the body and the point where it leaves the body (this intersection distance will be somewhat shorter, inasmuch as the shock wave is nearer to being normal to the flow than is the Mach wave). Also, the free-stream Mach number used was not exactly the tunnel Mach number, inasmuch as the region in which the pressures were measured was behind a conical shock wave from the nose of the cylindrical body. For this reason, the free-stream Mach number was taken to be 1.87. The value of the free-stream Mach number is probably much less in doubt than the shock deflection, since this was determined by measuring the shock angle with respect to the surface of the cylindrical body. Any flow inclination or any movement of the body would cause the determination of the deflection angle to be false. Also note that the pressure ratio across the shock is more sensitive to a change in deflection than it is to a change in Mach number. The errors are more serious at the lower deflection angles, so that although the linearized theory should give better results here, it may be that the experimental and theoretical curves are not actually for the same flow conditons (δ may be different for the reasons mentioned).

It is clear, however, that the sharp-peaked pressure curve is more closely followed by the experimental points for $\delta = 4°$ than for $\delta = 11.2°$. On the lee side the form of the experimental and theoretical curves is nearly the same but they are shifted with respect to each other due to the boundary-layer effects.

From the velocity components the angle the streamlines make with the generators of the cylinder can be computed easily, and it is found at the $\theta = 90°$ station that the flow deflection is 4° for $\delta = 4°$ and 12-1/2° for $\delta = 11.2°$, while from the china-film pictures in Ref. 8 these angles

are found to be approximately 25° and 45°, which substantiates the statements made about the experimentally determined cross-flow as compared to the theoretical cross-flow. The angle of cross-flow is seen experimentally to remain larger than predicted by the asymptotic theory, although it does decrease appreciably as we move downstream from the shock wave.

APPENDIX A

THE FUNCTIONS $W_1(Z')$ AND $W(Z')$

z'	W_1	W_3
0	.500	.500
.2	.514	1.139
.4	.509	1.392
.6	.490	1.310
.8	.463	1.007
1.0	.430	.606
1.2	.382	.222
1.4	.356	- .081
1.6	.315	- .262
1.8	.277	- .329
2.0	.241	- .296
2.2	.207	- .212
2.4	.174	- .112
2.6	.146	- .014
2.8	.120	.055
3.0	.097	.003
3.2	.077	.099
3.4	.059	.084
3.6	.044	.057
3.8	.031	.023
4.0	.021	- .008

REFERENCES

1. C. Ferrari, "Interference Between Wing and Body at Supersonic Speeds — Theory and Numerical Application" , J. Aero. Sci., 15, No. 6, 317 (June, 1948).

2. J. Nielsen and F. Matteson, "Calculation Mehtods for Estimating the Interference Pressure Field at Zero Lift on a Symetrical Swept-Back Wing Mounted on a Circular Cylindrical Body," NACA RM A9E19, 1949.

3. J. Nielsen, "Supersonic Wing-Body Interference," California Institute of Technology Thesis.

4. C. Ferrari, "Interference Between Wing and Body at Supersonic Speeds — Part III, Numerical Application of Linear Theory," CAL/CM — 463, April, 1951.

5. W. Pell, "Monograph VIII. Lifting Surfaces in Supersonic Flow - Part II. Linearized Three-Dimensional Theory," Technical Report No. 102-AC49/8-100, Wright-Patterson Air Force Base.

6. E. Migotsky and M. Morkovin, "Three-Dimensional Shock-Wave Reflections," J. A. S., 18, No. 7, 484 (July, 1951).

7. E. Migotsky, "On the Reflections of Shock Waves in Three-Dimensions," Ph. D. Thesis, University of Michigan, April, 1951.

8. M. Morkovin, E. Migotsky, H. Bailey, and R. Phinney, "Experiments on Interaction of Shock Waves and Cylindrical Bodies at Supersonic Speeds," J. A. S., 19, No. 4, 237 (April, 1952).

9. G. Morikawa, "The Wing-Body Problem for Linearized Supersonic Flow," Progress Report No. 4-116, Jet Propulsion Laboratory, California Institute of Technology, Dec., 1949.

10. W. Hayes, "Linearized Supersonic Flow," North American Aviation Company Report No. AL-222, 1947 .

11. P. Lagerstrom and M. Van Dyke, "General Considerations About Planar and Non-Planar Lifting Systems," Douglas Aircraft Company, Report No. SM-13432, 1949.

12. R. V. Churchill, Fourier Series and Boundary-Value Problems, McGraw-Hill, 1941.

13. T. Von Karman and N. Moore, "Resistance of Slender Bodies Moving with Supersonic Velocities," Trans. A.S.M.E., 54, 303 (1932).

14. Dailey, C. L., and Wood, F. C. Computation Curves for Compressible Fluid Problems, John Wiley and Sons, Inc., 1949.